补充资料
Supplementary Information

自下而上的克级石墨烯的合成
Gram-scale bottom-up flash graphene synthesis

Duy X. Luong,[1,2] Ksenia V. Bets,[3] Wala Ali Algozeeb,[2] Michael G. Stanford,[2] Carter Kittrell,[2] Weiyin Chen,[2] Rodrigo V. Salvatierra,[2] Muqing Ren,[2] Emily A. McHugh,[2] Paul A. Advincula,[2] Zhe Wang,[2] Mahesh Bhatt,[4] Hua Guo,[3] Vladimir Mancevski,[2] Rouzbeh Shahsavari,[4,5*] Boris I. Yakobson,[2,3,6*] and James M. Tour[2,3,6*]

[1]Applied Physics Program, [2]Department of Chemistry, [3]Department of Materials Science and NanoEngineering,

Rice University, 6100 Main Street, Houston, Texas 77005, USA

[4]C-Crete Technologies, 13000 Murphy Rd, Unit 102, Stafford, TX 77477, USA

[5]Department of Civil and Environmental Engineering, [6]Smalley-Curl Institute and the NanoCarbon Center,

Rice University, 6100 Main Street, Houston, Texas 77005, USA

智科眼【https://www.zhisci.com】英文PDF论文，一键免费变中英双语对照！

设备
Equipment

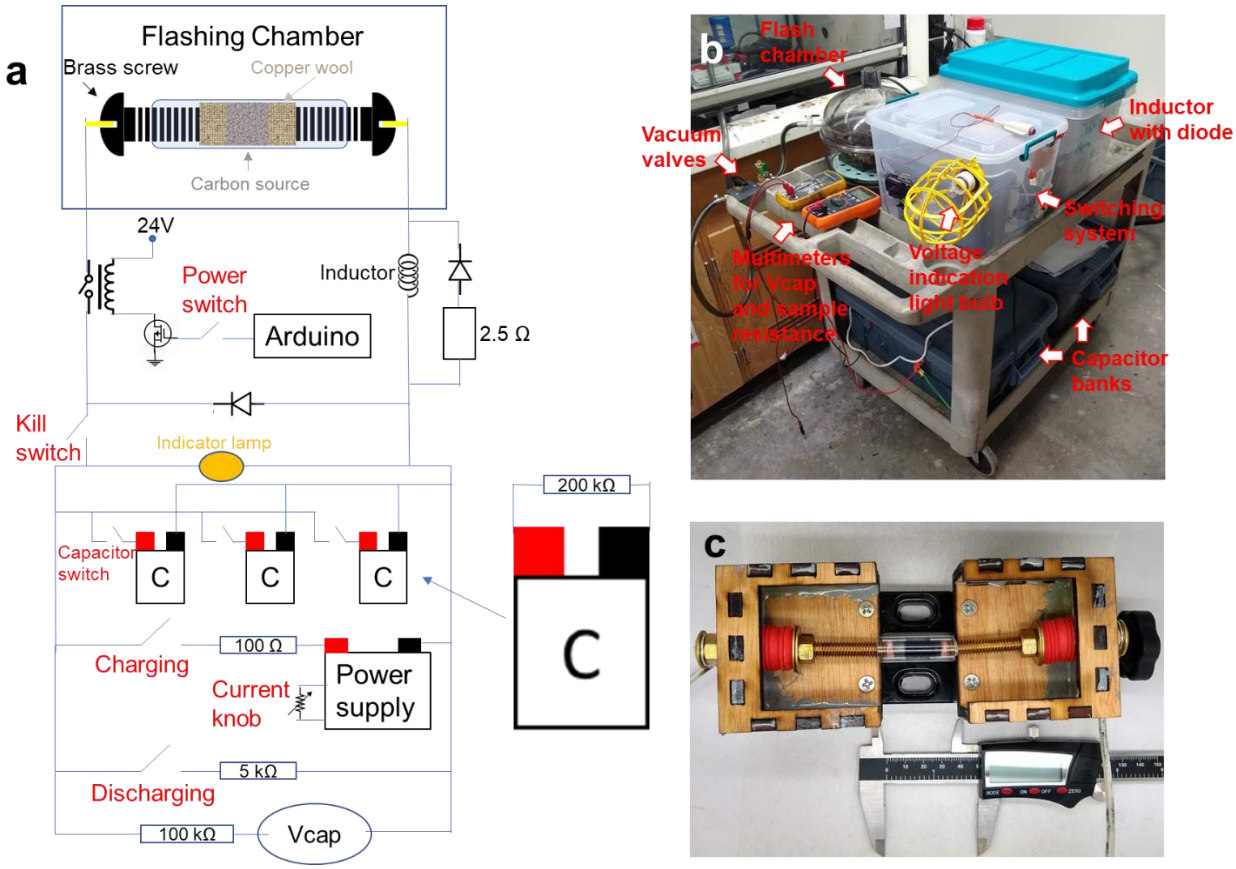

补充图1.FJH系统. FJH系统的电气原理图. 在塑料车上
Supplementary Fig. 1. FJH system. **a**. Electrical schematic of the FJH system. **b**. Photograph of
设置的系统的照片. 样品架由一个小型商用虎钳(亚马逊)和激光切割的木制
the system set up on a plastic cart. c. The sample holder that is made from a small commercial
部件制成. 松配合的黄铜螺钉(在闪光时允许气体逸出)起
vise (Amazon) and laser cut wooden parts. The loosely fitting (to permit gas escape during
到两个电极的作用,接触到接触所需碳源的铜毛塞(或石墨盘).
flashing) brass screws act as two electrodes that contact the copper wool plugs (or graphite disks)
红色橡胶塞可逐渐压缩样品,
that touch the desired carbon source. Red rubber stoppers provide gradual compressing of the

智科眼【https://www.zhisci.com】英文PDF论文，一键免费变中英双语对照！

而当老虎钳被压缩以增加样品的导电性 卡尺宽度为5
sample while the vice is compressed to increase the conductivity of the sample. Caliper width is
厘米.
5 cm.

FJH组件列表：
FJH Components list:

电容器：10x 450 V, 6 mF铝电解电容器
- Capacitor: 10x of 450 V, 6 mF aluminum electrolytic capacitors (Mouser #80-

该电容器组用于批量为≤0.5g。
PEH200YX460BQU2). This capacitor bank is for FG synthesis with batch sizes ≤0.5 g

10x 400v, 18mF铝电解电容器(Mouser#80-ALS70A183QS400)
- 10x of 400 V, 18 mF aluminum electrolytic capacitors (Mouser # 80-ALS70A183QS400).

此附加电容器组用于批量>0.5 g且≤1.0 g的FG合成
This additional capacitor bank is for FG synthesis with batch sizes >0.5 g and up to 1.0 g

机械继电器：900 V,500 A(TE连接性LEV200A5ANA)
- Mechanical relay: 900 V, 500 A (TE Connectivity LEV200A5ANA)

电源：LED电源299.6W 214-428V 700mA
- Power supply: LED Power Supplies 299.6W 214-428V 700mA (Mouser # 709-

电流旋钮是一个10 kΩ电位计
HLG320H-C700B). Current knob is a 10 kΩ potentiometer

-Vcap由万用表Fluke 189测量
- Vcap is measured by a multimeter Fluke 189

-放电和充电开关断路器：400 V, 6A(ABB S 282 K 6A)
- Discharging and charging switch breaker: 400 V, 6A (ABB S 282 K 6A)

-电容开关断路器：277V, 10A(ABB S201P-C10)
- Capacitor switch breaker: 277 V, 10 A (ABB S201P-C10)

-压井开关断路器：440 V, 63 A(AAB S283 UC Z 63A)
- Kill switch breaker: 440 V, 63 A (AAB S283 UC Z 63A)

-控制器：Arduino Uno, 带LCD显示屏
- Controller: Arduino Uno with LCD display

-感应器：24 mH(鼠标553-C-80U)
- Inductor: 24 mH (Mouser #553-C-80U)

-二极管：1200 V, 560 A(Mouser#747-MDO500-12N1)
- Diode: 1200 V, 560 A (Mouser #747-MDO500-12N1)

注意：存在触电甚至触电的危险, 因此应实施这些功能.
CAUTION: There is a risk of electrical shock or even electrocution, so these features

此列表并非全面的, 而是说明了将风险降至最低所需的协议.
should be implemented. This list is not intended to be comprehensive but demonstrative of

the protocols needed to minimize risk.

封闭或小心绝缘所有电线连接.
1. Enclose or carefully insulate all wire connections.

智科眼【https://www.zhisci.com】英文PDF论文，一键免费变中英双语对照！

所有连接、电线和部件必须适用于高电压和高电流.

2. All connections, wires and components must be suitable for the high voltages and currents.

请注意, 组件故障可能会导致意外位置出现高电压, 例如开关晶体管上的散热器.

3. Be aware that component failure could cause high voltage to appear in unexpected places, such as heat sinks on the switching transistors.

控制线应具有额定高电压的光电隔离器.

4. Control wires should have opto-isolators rated for high voltage.

提供一个可见的充电指示器. 230V透明玻璃白炽灯泡是一个不错的选择, 因为灯

5. Provide a visible charge indicator. A 230 V clear glass incandescent light bulb is a good

丝上的辉光也提供了电容器组上电荷量的近似指示器.

choice as the glow on the filament also provides an approximate indicator of the amount

强光=危险！

of charge on the capacitor bank. Bright light = danger!

不要将拨动开关与金属拨动开关一起使用. 如果形成电弧, 金属开关可能带电.

6. Do not use toggle switches with metal toggles. If an arc develops, the metal toggle could become charged.

一手规则. 在系统上工作时, 只使用一只手, 另一只手不要接触任何接地表面.

7. One hand rule. Use only one hand when working on the system, with the other hand not touching any grounded surface.

在每个电容器上安装100000欧姆范围内的放电电阻器, 使电荷在~1小时内始终放电.

8. Install bleed resistors in the range of 100,000 ohms on each capacitor so that charge will always bleed off in ~1 h.

提供一个机械放电断路器开关, 该开关连接到几百欧姆的功率电阻器, 以快速释放

9. Provide a mechanical discharge circuit breaker switch connected to a power resistor of a

电容器的电荷.

few hundred ohms to rapidly bleed off the capacitor charge.

提供一个“灭弧”断路器开关, 从电容器组上断开样品架.

10. Provide a "kill" circuit breaker switch to disconnect the sample holder from the capacitor bank.

提供交流断路器开关.

11. Provide an AC disconnect circuit breaker switch.

在设备上张贴高压警告标志.

12. Post high voltage warning signs on the apparatus.

使用断路器作为开关. 断路器具有内置的消弧功能, 可中断1000安培

13. Use of circuit breakers as switches. Circuit breakers have built-in arc suppression that

或更多电流. 传统的开关没有如此高的消弧水平, 并且由于高电流

can interrupt 1000 amps or more. Conventional switches do not have such a high level of

脉冲会烧坏或焊接闭合.

arc suppression and can burn out or weld closed due to the high current pulses.

使用额定直流电压的断路器. 大多数交流断路器的直流额定电压为1/2或更

14. Use circuit breakers rated for DC voltage. Most AC circuit breakers have a DC rating 1/2
低, 因为直流电弧很难抑制. 为直流太阳能
the voltage or less, since DC arcs are much more difficult to suppress. Circuit breakers
电力系统设计的断路器是一个很好的选择.
designed for DC solar power systems are a good choice.

选择断路器时, 应根据0.1s的典型时间曲线而不是稳态电流额定值进行选择.

15. When choosing circuit breakers, choose by the time curves typical for 0.1 s, rather than
与额定电流相比, K型直流断路器在0.1s时的跳闸
the steady state current rating. K-type DC circuit breakers will have ~10x higher trip
电流将高出约10x, Z型断路器在0.1s时的跳闸电流将高出约4x.
current at 0.1 s compared to their rated current, and Z-type breakers will have ~4x higher
大多数断路器设计的“ 延迟跳闸 ”将允许比断路器的稳态额定值
trip current at 0.1 s. This "delayed trip" designed into most circuit breakers will allow
更高的脉冲电流.
much higher pulse currents than the steady state rating of the breaker.

在放电电路中包含少量电感, 以将上升时间限制在毫秒或更长.

16. Include a small amount of inductance in the discharge circuit to limit the rise time to a
极快的放电会损坏部件并对其他实验室设备造成射频干扰.
millisecond or more. Extremely fast discharges can damage components and cause RF

interference with other lab apparatus.

请记住, 系统可以在毫秒内放电数千焦耳, 这可能导致继电器甚至电容器等部件

17. Keep in mind that the system can discharge many thousands of Joules in milliseconds,
爆炸. 这
which can cause components such as relays or even capacitors to explode. These
些部件应密封, 以防止高压和可能的飞屑.
components should be enclosed to protect against both high voltage and possible flying

debris.

随时准备一个带有高压测试引线的电压表. 在电容器组上工作

18. Keep a voltmeter with high voltage test leads handy at all times. When working on the
时, 务必检查每个电容器组上的电压. 断线或松动的连接可能使电容器
capacitor bank, always check the voltage on each. A broken wire or loose connection
处于充电状态.
could leave the capacitor in a charged state.

使用本设备时, 请戴上厚橡胶手套, 以防触电.

19. Wear thick rubber gloves when using the apparatus to protect from electrocution.

所有用户都应接受有经验的电气技术人员的适当培训.

20. All users should be properly trained by an experienced electrical technician.

利用这些设计和安全参数, 实验室规模设备的商业化很可能随之而来.
Commercialization of laboratory-scale equipment will likely follow using these design and

safety parameters.

将高碳材料转化为FG的估算能量：
Estimated energy for conversion of high carbon materials into FG:

对于100 mg批次，一组电容为60 mF的电容器从220 V 150 V放电，然后
With 100 mg batch, a bank of capacitors with capacitance of 60 mF discharge from 220 V – 150 V, then

$$E = \frac{(V_1{}^2 - V_2{}^2) \times C}{2 \times M} = 7.2\ kJ \cdot g^{-1}$$

E： 每克能量
E: Energy per gram

V1和V2：分别为闪光前后的电压
V_1 and V_2: Voltage before and after flash, respectively

C： 电容
C: Capacitance

M： 每批质量
M: Mass per batch

拉曼光谱分析与涡轮层石墨烯的讨论
Discussion of Raman Analyses and Turbostratic Graphene

石墨烯被定义为二维材料
Graphene is defined as a 2-D material

虽然石墨烯通常被描绘成一层碳，但它只是在特殊的实验室条件下作为一层单独的碳片出现。
While graphene is often depicted as a single sheet of carbon, it occurs as a single isolated sheet only in specialized laboratory conditions. 在任何实质性的生产方法，如我们在这里报告，石墨烯将出现在聚集体的形式。
In any substantial production method such as we are reporting here, graphene will appear in the form of aggregates. 这一领域的先驱们将石墨烯定义为二维材料，而将碳纳米管定义为一维材料，将石墨定义为三维材料。
The pioneers in this field have defined graphene as a 2-D material, in contrast to carbon nanotubes as a 1-D material and graphite as a 3-D material.[1, 2, 3, 4] 当这些聚集体中的sp2碳板保持二维材料而不是三维材料的电子结构时，则使用描述性形容词作为前缀，如双层石墨烯、少层石墨烯、N层石墨烯。
When the sp^2-carbon sheets within these aggregates retain the electronic structure of a 2-D rather than 3-D material, then a descriptive adjective is used as a prefix, such as *bilayer graphene, few-layer graphene, N-layer graphene*. 如果AB堆叠(伯纳尔)，石墨烯是指当小于10层时使用的术语，因为与石墨相比，在小于10层时有明显的物理性质。
If AB-stacked (Bernal), then graphene is the term used when there are <10-layers since there are distinct physical properties, relative to graphite, at <10 layers. 只有在>9层时，才会产生石墨状的特性，并且只有相邻的片层是AB堆叠的。
Only at >9 layers, do graphite-like property ensue and only if the adjacent sheets are AB-stacked.[5] 当出现随机定向的分层而不是像FG那样的AB堆叠时，几个不同的形容词与相同的含义，如：方向错误，3扭曲，6旋转，7旋转断裂，8，9弱耦合，10和
When randomly oriented layering occurs rather than AB-stacked as in the case of FG, several different adjectives are used with the same meaning, such as: *misoriented*,[3] *twisted*,[6] *rotated*,[7] *rotationally faulted*,[8, 9] *weakly coupled*,[10] and

智科眼【https://www.zhisci.com】英文PDF论文，一键免费变中英双语对照！

涡轮层. 尽管术语不同,但许多作者一致认为,在这些情况下,当随机堆叠时,各个
turbostratic.[11] In spite of the varied terminology, there is agreement among many authors that in
层保留其二维特性. 因此,
these cases, the individual layers retain their 2-D properties when randomly stacked. Hence, the
即使存在许多层,科学文献也支持使用术语“石墨烯”来进行这种堆叠.
use of the term "*graphene*" for such stacking is supported in the scientific literature, even when
如我们将要展示的,拉曼光谱提供了对电子结构的直接监测,并且
there are many layers.[12] As we will show, the Raman spectrum provides a direct monitor for the
在识别这些聚集体的二维性质方面是毫无疑义的
electronic structure and is also unambiguous in identifying the 2-D nature of these aggregates.

构成二维材料的不是物理尺寸或原子层的数量,而是性质,特别是电子性质.
It is not the physical dimensions or the number of atomic layers but rather the properties,
石墨烯的特征是二维的狄拉克
especially electronic properties that constitute a 2-D material. Graphene is characterized by a 2-
费米子气体. 二维材料是电子迁移率高度各向异性的材料,正如碳纳米管是一维材料
D gas of Dirac fermions.[13] A 2-D material is that which is highly anisotropic in electron mobility,
一样,因为它在一个方向上的迁移率很高. 对于石墨烯,
just as carbon nanotubes are a 1-D material because high mobility in one direction. For graphene,
,在x-y平面上的迁移率是弹道的,但是当堆叠时,c轴的迁移率要小得多.
the mobilities are ballistic in the x-y plane, but when stacked, the c-axis mobility is very much
而涡轮层石墨烯的各向异性最大,即使多层石墨烯,在二维仍保持完全二维的
smaller. And turbostratic graphene has the greatest anisotropy of all, and even for multiple
弹道流动性,在三维则有许多数量级的电导率较低.
layers, it remains fully 2D with ballistic mobility in two dimensions, and many orders of

magnitude lower conductivity in the third dimension.

Kim等人的实验测量.证明了当石墨烯片以扭曲的方式堆叠时,平面内的弹道
Experimental measurements by Kim et al. demonstrate that the extremely large
电子和那些试图在层间交叉的电子之间的极大各向异性被保留.
anisotropy between ballistic electrons in plane and those trying to cross between layers is
他们报告了高有序热
retained when the graphene sheets are stacked in a twisted manner.[7] They report ~10^{-3} ohm-
解石墨(HOPG)的~10-3欧姆电阻率,比铜高出约5个数量级,层间电阻率又高出4个数量级.
meter resistivity for highly ordered pyrolytic graphite (HOPG) which is ~5 orders of magnitude

higher resistivity than copper and the interlayer resistivity is again 4 orders of magnitude larger.
涡轮层石墨烯的面内输运对电子来说仍然是弹道输运. 涡轮层石
The in-plane transport for turbostratic graphene remains ballistic for the electrons. Turbostratic
墨烯,即使有许多层,也确实是一种二维材料,电子在二维像无质量费米气体一样自由移动
graphene, even with many layers, is truly a 2-D material whereby electrons move with complete
,但实际上不能垂直于层移动.
freedom like a massless Fermi gas in two dimensions but are, in effect, unable to move
很少能找到像多层涡轮层状石墨烯那样纯二维的材料.
perpendicular to the layering. It is rare to find any other material that is so purely 2D as

multilayer turbostratic graphene.

拉曼光谱作为二维特征的决定性标准
Raman as a definitive standard for 2-D character

拉曼光谱已经成为石墨烯诊断的标准；这种工具几乎出现在所有的实验研究中.
Raman spectroscopy has become the standard as a diagnostic of graphene; that tool
4,7,8,9,12,14,15,16,17, 这是因为它是石墨烯
appears in almost every experimental study.[4, 7, 8, 9, 12, 14, 15, 16, 17] And that is because it is a direct
电子能带结构的直接检测标准, 而电子能带结构又在这种二维材料的独特特性中起着中心作用.
probe of the electronic band structure of the graphene, which in turn plays a central role in the
unique character of this 2-D material.

涡轮层石墨与涡轮层石墨烯
Turbostratic graphite vs. turbostratic graphene

涡轮层状石墨的D峰远大于G峰和2D峰, 这与优化的FG样品相反, 后者的D峰远小于G峰,
The D-peak of turbostratic graphite is much larger than both the G-peak and the 2D peak,
后者又小于2D峰.
which is opposite for an optimized sample of FG which has a D-peak that is very much smaller
拉曼光谱是原子结构振动运动的
than the G-peak, which in turn is smaller than the 2D peak.[18] Raman spectroscopy is a probe of
检测标准, 因此巨大的D峰证明了涡轮层石墨中单个石墨烯晶格是非常破碎的.
the vibrational motions of the atomic structure, hence the huge D-peak proves that the individual
它在纳米尺度上是极度无序的.
graphene lattice is very disrupted in turbostratic graphite. It is profoundly disordered on the
它不能再恢复为二维石墨烯材料. 由于难以获得这种材料,
nanoscale. It can no more be restored to a 2-D graphene material. Researchers have lamented
研究人员对涡轮层状石墨烯这一非常有前途的领域的研究进展缓慢表示遗憾.
the slow development of the field of research into the very promising area of turbostratic
涡轮层状石墨烯只有微量(
graphene due to the difficulty of obtaining the material.[8, 11] Turbostratic graphene was only
按重量)通过化学气相沉积或外延生长产生. 即使在这些精心控制
produced in trace amounts (by weight) by CVD or epitaxial growth. And even growth under
的生长条件下生长, 也不能保证材料是涡轮层状的.
these carefully controlled growth conditions, it does not assure that the material will be
一组人尝试用化学气相沉积法在镍箔上沉积10层涡轮层石墨烯, 得到了不同的结
turbostratic. One group that attempted a thickness of 10-layer turbostratic graphene using CVD
果, 有时是AB堆积, 有时是涡轮层, 有时是两者的混合物.
on nickel foil obtained varying results, sometimes AB-stacked, sometimes turbostratic, and
即使是这种最近发展起来的多层生长涡轮层石墨烯的工艺也很
sometimes a mixture of the two.[9] Even this recently developed process to multilayer growth of
难使其可靠.
turbostratic graphene has been difficult to make reliable.

层数不能确定二维特征
Number of layers does not define 2-D character

已有研究表明, 对于AB堆积石墨烯, 单层石墨烯(SLG)或少层石墨烯(FLG)的二维性质
Several authors have reported that for AB-stacked graphene, the 2-D properties of single-
随Raman光谱的变化逐渐向三维材料转变, 在约10层处转变为HOPG的二维性质.
layer graphene (SLG) or few-layer graphene (FLG) gradually transition to 3-D material with the
然而, 这
Raman spectra evolving into that characteristic of HOPG at about 10 layers.[3, 13] However, this
个经验法则不适用于涡轮层石墨烯, 因为各个层是弱耦合的, 所以它们保持了独立于层数
rule of thumb does not apply to turbostratic graphene because the individual layers are weakly
的二维特征.
二维
coupled, so they retain the 2-D character independent of the number of stacked layers.[7, 9] The 2D
峰保持其窄的洛伦兹线型, 在K点处狄拉克锥不引入附加态.
peak retains its narrow Lorentzian lineshape, and no additional states are introduced to the Dirac
因此, 2D峰的拉曼散射仍然是一个双峰共振增强的单峰, 这导致了它
cone at the K-point. Hence the Raman scattering for the 2D peak remains a single peak that is
的强增强.
它仍然是一个零带隙半
doubly resonance enhanced, giving rise to its strong enhancement. And it remains a zero band
导体.
相反, 当两个层是AB叠加时, 强耦合会在K点周围产生抛物线形状的
gap semiconductor. In contrast, when two layers are AB-stacked, the strong coupling creates
附加状态, 从而允许更多的跃迁.
additional states with a parabolic shape around the K-point, which allows for more transitions.
2D峰由四个洛伦兹峰、两个强峰和两个弱峰组成, 它在失去洛伦兹线形状的同时, 实质上变
The 2D peak becomes a sum of four Lorentzians, two strong and two weak, and it substantially
宽了.
有几位作者研究了旋转错配的石墨烯,
broadens while losing its Lorentzian line shape. Several authors have studied rotationally
有些是通过折叠单个薄片的方法来保证不对齐.
misoriented graphene, some by the method of folding a single sheet, which guarantees
由于2p原子轨道的重叠性很差, 这两个薄片保留了它们的SLG特性.
misalignment. As a result of the poor overlap of the 2p atomic orbitals, the two sheets retain
their SLG characteristics.[7, 9, 11]

某些相对较弱的拉曼组合带的存在或不存在是透层石墨烯发生的正标志：在1650cm-1
The presence or absence of certain relative weak Raman combination bands are positive
到2300cm-1的频率范围内, 随着拉曼2D模式的特征, 已生长的石墨烯的组合拉曼模式被用作
indicators for the occurrence of turbostratic graphene: “Combination Raman modes of as-grown
涡轮层石墨烯的特征.
graphene within the frequency range of 1650 cm^{-1} to 2300 cm^{-1}, along with features of the
有一个
Raman 2D mode, were employed as signatures of turbostratic graphene.” There is a
平面内横向声学(iTA)和纵向光学(LO)、iTA和纵向声学(LA)以及LO+LA模式的组合.
“combination of in-plane transverse acoustic (iTA) and the longitudinal optic (LO), iTA and
这里, 我们将iTALO模式指定为TS1, 将
longitudinal acoustic (LA) and LO + LA modes. Here, we designate the iTALO− mode as TS_1
iTOLA/LOLA模式指定为TS2.11个
and the iTOLA/LOLA modes as TS_2.”[11]

智科眼【https://www.zhisci.com】英文PDF论文，一键免费变中英双语对照！

使用TS1和TS2作为正指标

Using TS_1 and TS_2 as positive indicators

我们将使用TS1和TS2的名称来表示这两个仅对SLG和涡轮层石墨烯具有拉曼活性的特征.

We will use the designations of TS_1 and TS_2 to indicate these two features that are Raman active only for SLG and turbostratic graphene. TS_1 is a single Lorentzian that occurs in the vicinity of 1880 cm^{-1} and TS_2 consists of two closely space Lorentzians that occurs in the vicinity of 2030 cm^{-1}; however, it must be kept in mind that these lines exhibit dispersion, like many Raman features in graphene. The excitation wavelength must always be noted, and dispersion corrections applied when comparing the peak frequencies.

TS1是发生在1880cm-1附近的单个洛伦兹线, TS2由发生在2030 cm-1附近的两个紧密空间洛伦兹线组成；但是, 必须记住, 这些线表现出色散, 就像石墨烯中的许多拉曼特征一样.

必须始终注意激发波长, 并在比较峰值频率时应用色散校正.

消失的M带

The silent M band

此外, “ M ”带出现在1750cm-1左右, 但对于涡轮层状石墨烯, 这种组合带变得消失。

In addition, the "M" band occurs about 1750 cm^{-1} but this combination band becomes silent for turbostratic graphene. Hence the presence of the M band is a negative indicator for turbostratic graphene, and a positive indicator for AB-stacked graphene as well as HOPG.

因此, M带的存在对于涡轮层石墨烯是一个负的指标, 对于AB堆叠石墨烯和HOPG是一个正的指标.

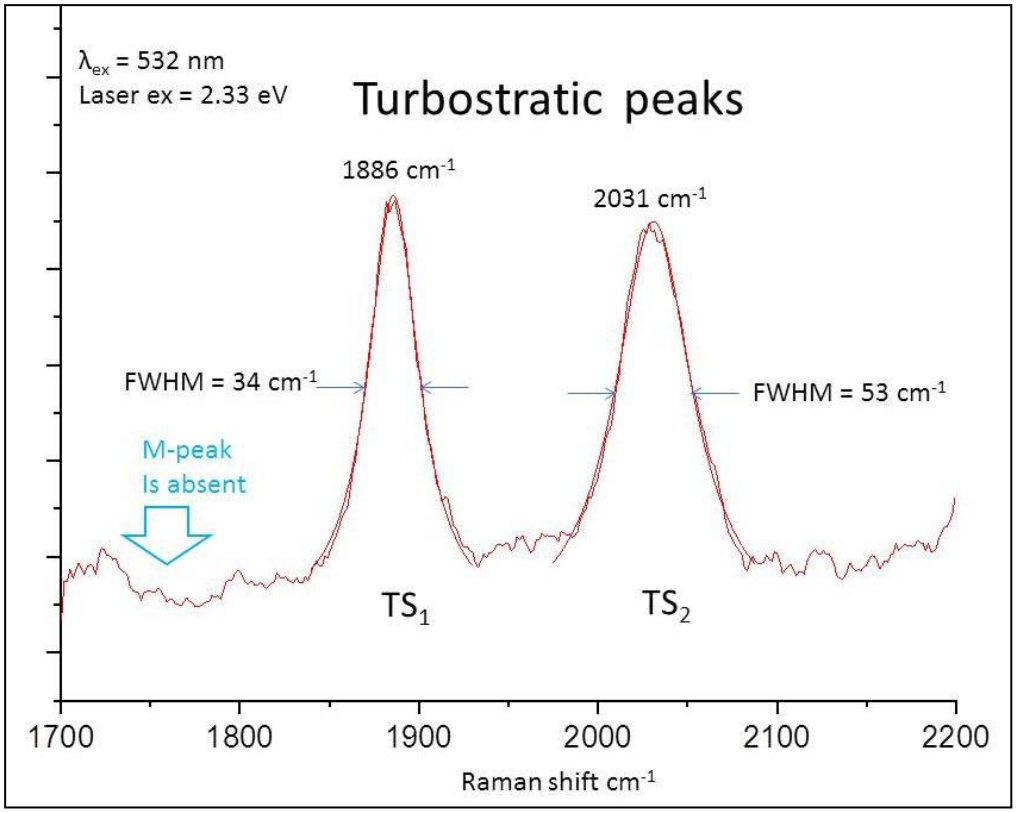

补充图2.CB-FG拉曼光谱中的涡轮层峰.

Supplementary Fig. 2. Turbostratic peaks in the Raman spectrum of CB-FG. $I_{G/TS1}$ ~30. 洛伦兹拟合显示为叠加平滑线. TS1的R平方为0.994, TS2的R平方为 Lorentzian fit is shown as a superimposed smooth line. The R-squared is 0.994 for TS_1 and 0.99 这些极好的拟合表明了FG的高质量, 并且这些拉曼线的明显存在归因于涡轮层石墨 for TS_2. These excellent fits indicate the high quality of the FG and the unmistakable presence 烯. of these Raman lines are attributable to turbostratic graphene.

智科眼【https://www.zhisci.com】英文PDF论文，一键免费变中英双语对照！

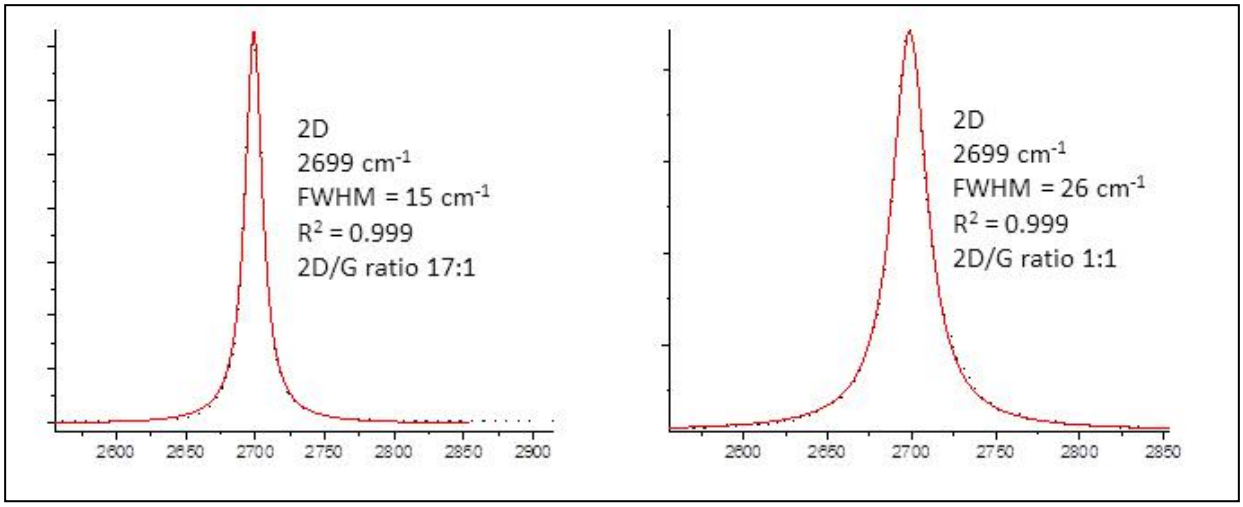

补充图3. CB-FG拉曼光谱中的2D峰. 左：CB-FG中的最佳点,

Supplementary Fig. 3. 2D peak in the Raman spectrum of CB-FG. Left: best point in CB-FG,

右：CB-FG中的代表点. 两个峰都显示出近乎完美的洛伦兹线形状.

right: representative point in CB-FG. Both peaks exhibit nearly a perfect Lorentzian line shape.

黑点是理论上的线型. 两个峰的相关系数R2均为0.999.

The black dots are the theoretical line shape. The R^2 for the correlation is 0.999 for both peaks.

这表明在K点有一个完全锥形的狄拉克锥. 异常大的I2D/G也表明多层涡

This is indicative of a fully conical Dirac cone at the K-point. The exceptionally large $I_{2D/G}$ is

轮层状石墨烯, 正如一些研究人员指出

also indicative of multilayer turbostratic graphene, as several researchers point to an increasing

$I_{2D/G}$.[7, 11]

窄的单一洛伦兹2D峰只能出现在SLG或涡轮层石墨烯中, 由此相邻层被分离并且不

The narrow, single Lorentzian 2D peak can occur only for either SLG or turbostratic

会产生额外的电子态.

graphene whereby the adjacent layers are decoupled and do not give rise to additional electronic

这反过来意味着它保持完美的二维空间, 即使有许多层石墨烯堆叠.

states. This in turn means that it remains perfectly 2-dimensional, even though there are many

对于图3左边的最佳例子, 洛伦兹半最大全宽度(FWHM)实际上变

layers of graphene stacked. For the best example on the left of Fig. 3, the Lorentzian full-width-

得比完美SLG窄.

at-half-maximum (FWHM) has actually become narrower than for the perfect SLG. This

这种变窄是旋转错配石墨烯的一个独特特征, 它是堆叠的, 并且只发生在涡轮层状石墨烯上,

narrowing is a unique feature of rotationally misaligned graphene that is stacked and only occurs

如下面相对于其他报告所述. 我们观察到二维峰窄至

for turbostratic graphene, as describe below relative to other reports. We have observed 2D peaks

15cm-1, 仅出现在多层涡轮层石墨烯中. 宽得多

as narrow as 15 cm^{-1}, which occurs only for multiple layers of turbostratic graphene. The much

的波段是伯纳尔双层的, 它是四个峰的总和, 显然是非洛伦兹的.

broader band is for a Bernal bilayer, which is a sum of four peaks and is clearly non-Lorentzian.

CB-FG与报道的涡轮层状石墨烯拉曼光谱的比较
Comparison of the Raman spectrum of CB-FG to those in reported turbostratic graphene
补充表1:2D、TS1和TS2峰值与以往研究的比较.
Supplementary Table 1: Comparison of 2D, TS_1 and TS_2 peak with previous studies. The
在本研究中,我们修正了先前使用514nm激发激光的研究中的峰值位置,使之与532nm激发激
peak position from previous studies that used 514 nm excitation laser are corrected to match the
光相匹配.
532 nm excitation laser in this study.

	2D		TS_1		TS_2	
	Position	FWHM	Position	FWHM	Position	FWHM
Niilisk *et al.*[9]	2697	36	1886	34	2030	54
Garlow *et al.*[11]	2702	27	1884	38	2031	51
CB-FG	2699	15-26	1886	34	2031	53

将CB-FG光谱与两个不同参考文献中的数据进行比较
Comparing CB-FG spectra with data from two different references, the locations and
在这两种情况下,两个TS(涡轮层)峰的半高宽基本相同. 2D峰的位置
FWHM of the two TS (turbostratic) peaks are essentially identical in both cases. The location of
也相同,CB-FG-Lorentzian与Garlow等人的窄半高宽相匹配.
the 2D peak is also the same, with the CB-FG Lorentzian matching the narrower FWHM in that
我们观察到二维峰窄至15cm-1,仅出现在多层涡轮层石墨烯中.
from Garlow *et al.* We have observed 2D peaks as narrow as 15 cm^{-1}, which occurs only for
与Niilisk等人的6层涡轮层状石墨烯相比,在频率
multiple layers of turbostratic graphene. Comparing to Niilisk *et al.*, which has up to 6 layers of
和宽度上与TS1和TS2峰几乎相同.
turbostratic graphene, again there is a near identical match with the TS_1 and TS_2 peaks both in
对于文献和我们的CB-FG,都没有AB堆叠石墨烯和HOPG的M峰。
frequency and width. And for both references and our CB-FG, the M-peak which is
因此,在turbostratic
characteristic of both AB-stacked graphene and HOPG, is absent. Therefore, there are several
CB-FG拉曼光谱数据和从已证实的turbostratic石墨烯中获得拉曼光谱的两个参考文献之间
precise and redundant spectral feature alignments between the turbostratic CB-FG Raman data
存在一些精确且冗余的光谱特征比对.
and two references that have obtained Raman spectra from proven turbostratic graphene. In
此外,二维洛伦兹半高宽的变窄进一步支持了作为二维材料的涡轮层叠.
addition, the narrowing of the 2D Lorentzian FWHM is further support of the turbostratic
stacking as a 2-D material.

智科眼【https://www.zhisci.com】英文PDF论文,一键免费变中英双语对照!

很小的D带

The very small D-band

有趣的是, 并不是所有的边都表现为缺陷；因此它们并不总是显示D带.

Interestingly, not all edges behave as defects; hence they will not always display a D-band. For

对于锯齿形边缘, 产生D带的声子保持很低. 由于锯齿形边缘是自

the zigzag edge, the phonon that gives rise to the D-band remains silent. Since the zigzag edge is

由生长石墨烯最可能的边缘, 因此边缘的声子可以保持很低, 因此D-带仍然非常小.

the most probable edge for freely growing graphene then that phonon for the edges can remain

这在Yan等人的实验中得到了验证.做

silent, thus the D-band remains very small as observed. This was experimentally verified when

了一个完整的六角单晶石墨烯的拉曼图谱, D-带的边缘仍然很小.

Yan et al. did a thorough Raman map of their large hexagonal single-crystal graphene and the D-band remained very small at the edges.[19]

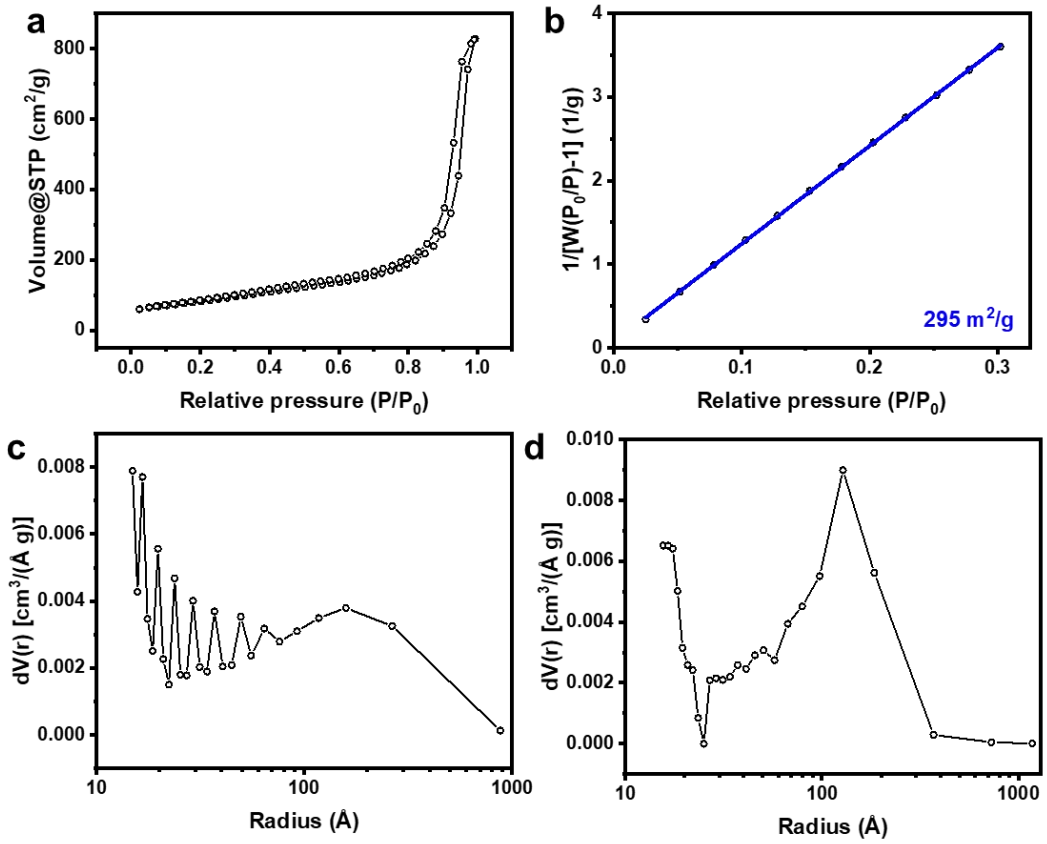

补充图4.CB-FG的BET比表面积分析. 等温线. 比表面积拟合

Supplementary Fig. 4. **BET surface area analysis of CB-FG.** a. Isotherm. b. BET surface area

吸附解吸孔径分布.

fitting. c-d. Absorption and desorption pore size distribution.

智科眼【https://www.zhisci.com】英文PDF论文，一键免费变中英双语对照！

补充表2：图1中各种材料的FJH参数.持续时间是开关打开时间, 而不是真正的闪光持续时间
Supplementary Table 2: FJH parameters for various materials in Fig. 1. Duration is the switch
. 电压行中的蓝色表示无闪光的预处理, 红色表示
opening time, not the real flash duration. Blue colors in the voltage row signify pre-treatment
合成过程中的实际闪光. 预处理是将材料部分
without a flash, red colors signify an actual flash during the FG synthesis. The pre-treatment is to
炭化, 以减少挥发性物质, 提高电导率.
partially char the material to reduce the volatile material and increase the conductivity. The
通过拉曼分析, 炭化过程只提供非晶材料. 这种预处理对于低
charring process affords only amorphous material by Raman analysis. This pre-treatment is
碳原料至关重要. 这种预炭化可以用选矿材料来消除,
crucial for starting materials with low carbon content. This pre-charring can be obviated with a
其中有一个预热循环, 因为当加热到一定温度以下时, 工业加热比用电便宜.
beneficiation material wherein there is a pre-heat cycle since industrial heating is less expensive
此外, 我们还列出了一种选
than using electricity when heating below certain temperatures. And we also list a beneficiation
矿材料, 橡胶轮胎衍生炭黑, 其中的挥发物在工业上被清除, 留下碳残留物(见橡胶材料一节）。
material, rubber tire-derived carbon black, where the volatiles were industrially removed, leaving
).
a carbon residue (see the rubber materials section).

原材了 **Starting 料 material** 炭黑(黑珍	重量 **Weight (mg)**	管子 **Tube (mm)**	电容 **Capacitance (mF)**	阻力 **Resistance (Ω)**	电压 **Voltage** 预处理 **Pretreat** 闪光 **Flash**	持续时间 **Duration (ms)**	成果材料 **Result material** CB-FG(最高
Carbon black 珠2000, (Black Pearls 卡博特) 2000, Cabot)	30	4	60	1.5	35 V x 5 110 V	500 50	CB-FG (highest $I_{2D/G}$) CB-FG(塑料
	120	8	60	1	60 V x 5 220 V	500 500	CB-FG (plastic 复合) compounding) CB-FG(1.1g
旧咖啡渣	1200	15	220	1.5	100 V x 5 250 V	500 500	CB-FG (1.1 g 批) batch)
Used coffee /CB grounds/ CB	1000	10	220	1000-3000	150 V x 3	10000	Charred coffee grounds

智科眼【https://www.zhisci.com】英文PDF论文，一键免费变中英双语对照！

(5%) (星巴克和 (Starbucks and 折叠式) Folgers) 烧焦的咖啡							
Charred coffee 渣 grounds 无烟煤	50	4	60	5-10	40 V x 5 130 V	50	C-FG
Anthracitic coal (费舍尔科学 (Fisher Scientific S98806) 煅烧焦炭	80	4	60	2000-3000	150 V	10000	Anthracite-derived FG 煅烧焦化烟
Calcine coke (牛弓 (Oxbow 煅烧 Calcining 国际, International, CPC 1400) CPC 1400)	80	4	60	0.8	80 V x 5 175 V	100 500	Calcined coke- 气 derived FG

闪光石墨烯形态

Flash Graphene Morphology

大多数有机化合物在高温退火时会石墨化. 在石

Most organic compounds will graphitize when annealed at elevated temperature. During

墨化过程中, 有机物被加热, 通过热解增加碳含量.

the graphitization process, an organic material is heated, increasing carbon content via pyrolysis.

在热解过程中, 碳与邻近的碳原子形成sp2杂化共价键, 并结晶成石墨的层状结构域.

During pyrolysis, the carbon forms sp^2-hybridized covalent bonds with neighboring carbon

非碳元素在极端温度下挥发.

atoms and crystallizes into layered domains of graphite. Non-carbon elements volatilize at the

然而, 石墨化材料的结构在很大程度上取决于制备方法和原料.

extreme temperatures. However, the structure of graphitized material largely depends upon the

最早对碳石墨化的各种形态进行批

method of preparation as well as the starting material. Some of the earliest work to critically

判性评论的是罗莎琳德富兰克林

comment on the various morphologies of carbon graphitization was that of Rosalind Franklin,[20]

智科眼【https://www.zhisci.com】英文PDF论文，一键免费变中英双语对照！

纯粹通过x射线衍射和密度测量来研究形貌.
which studied morphologies purely by means of x-ray diffraction and density measurements. It
人们注意到, 将几种非石墨碳加热到1700至3000°C之间后, sp2杂化碳层将定向成相对致密的
was noted that after heating several non-graphitic carbons to temperature between 1700 and 3000
结晶石墨. 这
°C, layers of sp^2-hybridized carbon would orient into relatively dense crystalline graphite. These
些被称为石墨化碳. 其它碳源材料在退火时会形成平行的多孔石墨层, 而不会
were termed *graphitizing carbons*. Other carbon starting materials would form porous graphite-
沿c轴扩展堆积. 这些
like layers in parallel groups when annealed, without extended stacking along the c-axis. These
被称为非石墨化碳.
were termed as *non-graphitizing carbons*.

随着原子分辨显微镜技术的发展, 石墨化和非石墨化炭的结构可以被可视化, 从而进
With the advent of atomic resolution microscopy techniques, the structure of *graphitizing*
一步揭示其形貌. 高
and *non-graphitizing carbons* could be visualized to further reveal their morphologies. High
分辨率TEM图像显示, 非石墨化碳, 如聚偏二氯乙烯和炭黑, 可能形成结构类似富勒烯
resolution TEM images have shown that non-graphitizing carbons, such as polyvinylidene
的封闭碳纳米颗粒, 21, 类似于手稿图3d中报道的闪蒸石墨烯的模拟结构.
chloride and carbon black, may form closed carbon nanoparticles which are fullerene-like in

structure,[21] and resemble the simulated structure of flash graphene reported in Figure 3d of the
这些粒子的特征是在所有的边上都有晶格条纹, 这表明它是一个三维的富勒烯状结
manuscript. These particles are characterized by lattice fringes along all sides, which suggest a 3-
构. 研究表明, 石墨化炭黑可以形成碳的类富勒烯多面体, 其
D fullerene-like structure. Work by Iijima reveals that graphitized carbon black can form
厚度为单层到几层. 它们被命名
fullerene-like polyhedra of carbon which are single to few layers in thickness.[22] These were
为石墨烯多面体. 这些结构的特征是沿石墨烯多面体边缘约120±20o的角度, 表明存
named graphene polyhedra. These structures are characterized by angles of ~ 120 ± 20° along the
在一些弯曲所需的5-7个成员环.
edge of the graphene polyhedra and suggest the presence of some 5-7 member rings required for
后来, Dresselhaus等人.用透射电镜观察了焦耳加热非晶碳的实时石墨化过程.
bending. Later, Dresselhaus et al. observed the real-time graphitization of amorphous carbon
特别值得注意的是, 石墨烯多面
via Joule heating in a transmission electron microscope.[23] Of particular interest, formation of
体粒子的形成是在焦耳加热下观察到的, 石墨壳层的厚度随着退火时间的增加而增加.
graphene polyhedra particles are observed upon Joule heating, with the thickness of the graphitic
王等人的其他工作.结果表明, 碳纳米纤维的石墨化和
shell increasing with annealing time. Other work by Wang et al. demonstrated that the electro-
剥落可以得到石墨烯. 24然而, 拉曼分
graphitization and exfoliation of carbon nanofibers can be afford graphene.[24] However, Raman
析显示石墨化后石墨烯的质量相对较差.
analysis reveals a relatively poor quality of graphene by electrographitization.

在这项工作中,可以发现石墨烯的各种形态,从石墨烯片到石墨烯多面体,如
In this work, various morphologies of graphene can be found ranging from sheets of
手稿的图1所示.
graphene to graphene polyhedra, as shown in Figure 1 of the manuscript. These morphologies
这些形貌在很大程度上取决于碳起始材料,它反映了起始材料是石墨化碳还是非石墨化碳;然而,在FG过程中,
largely depend upon the carbon starting material which reflects whether the starting material is a
加热和冷却发生在毫秒的时间尺度上.
graphitizing or *non-graphitizing* carbon; however, unique to the FG process, heating and cooling
快速的加热和冷却速度阻止了石墨烯层的堆积形成
occurs over the timescale of milliseconds. Fast heating and cooling rates prevent the stacking of
石墨,同时也阻止了石墨烯层的旋转对齐,从而产生涡轮层石墨烯.
graphene layers to form graphite, and it also prevents the rotational registration of graphene
这就产生了光谱上观察到的特殊石墨烯质量.
layers thus resulting in turbostratic graphene. This gives rise to the exceptional graphene quality
所有闪蒸的碳源至少呈现出石墨烯多面体类型的一些形貌.
observed spectroscopically. All carbon sources that were flashed exhibited at least some
手稿中的图1显示,本研究中的闪
morphologies which are of the graphene polyhedral type. Figure 1 from the manuscript shows
光石墨烯可以具有与文献中提到的类似的多面体结构,许多边角范围为109 -130 °.
that flash graphene in this work can have a similar polyhedron structure to that mentioned in
多面体通常由<5层组成,
literature with many edge angles ranging from 109 – 130°. The polyhedra are commonly
构成FLG分类.
然而,一些碳原料在焦耳加
composed of <5 layers which constitutes classification as FLG. However, some carbon starting
热时也会形成薄片.
我们的闪光石墨烯形态总结见
materials will also form sheets when Joule heated. A summary of our flash graphene
补充表S2.尽管没有针对所有的起始材料进行优化,但无烟煤、咖啡、生物炭、煅烧焦炭和松
morphologies can be found in Supplementary Table S2. Though not optimized for all the starting
木等材料形成石墨烯薄片.
materials, materials such as anthracite coal, coffee, biochar, calcined coke, and pine form
这与我们在文献报告中发现的形成石墨烯片的所有FG碳源以前都被归类为石
graphene sheets. This is consistent with the finding that that all of our FG carbon sources which
墨化碳的发现是一致的(补充表S2).
form graphene sheets have formerly been classified as *graphitizing carbon* in literature reports
因此,FG的形貌在很大程度上取决于起始碳源.
(Supplementary Table S2). Hence, the resultant morphology of FG largely depends on the
被归类为石墨化碳的材料,在热退火时容易热解为石墨,通常在闪蒸
starting carbon source. Materials classified as *graphitizing carbons,* which will readily pyrolyze
时会导致石墨烯片的部分形成.
into graphite when thermally annealed, generally result in the partial formation of graphene
石墨化和非石墨化碳材料在闪蒸过程中都会形成石墨烯多面体.
sheets when flashed. Materials classified as *graphitizing* and *non-graphitizing carbons* all result
这表明与FJH相关的快速
in the formation of graphene polyhedra during the flashing process. This suggests that the rapid
加热和冷却速度有效地延缓了
heating and cooling rates associated with FJH effectively retards further crystallization of the

智科眼【https://www.zhisci.com】英文PDF论文,一键免费变中英双语对照!

石墨烯多面体进入石墨结构域,从而产生独特的结构,这种结构通常不存在于经过相对缓慢
graphene polyhedra into graphitic domains, thereby giving rise to unique structures not typically
加热和冷却的石墨化材料中.
found in furnace-heated graphitized material which undergo a relatively slow heating and
FG结构是由超高纯度、低缺陷的材料组成的,这些材料会产生特殊的拉曼信号,如
cooling. FG structures are composed of ultra-high purity, low defect material which give rise to
高达17的I2D/G比.
exceptional Raman signatures, such as a $I_{2D/G}$ ratio of up to 17.

补充表3.从每个碳源形成闪光石墨烯时,石墨烯多面体或石墨烯片的存在情况表.
Supplementary Table 3. Table reporting the presence of graphene polyhedra or graphene
文献比较
sheets when forming flash graphene from each carbon source. Comparison to literature
表明石墨化碳(已知在热解时形成石墨)导致石墨烯片的形成.
shows that *graphitizing carbons* (which are known to form graphite upon pyrolysis) result in
所有闪蒸材料都呈现出石墨烯多面体.
formation of graphene sheets. All flashed materials exhibit some graphene polyhedral.

碳源 **Carbon Source**	**Graphene polyhedra**	**Graphene sheets**	**Pyrolysis morphology in references**
炭黑 Carbon black	Yes	No	Pyrolysis forms graphene polyhedra[20, 25]
Calcined petroleum coke	Yes	No	Pyrolysis forms crystalline graphite domains[20]
咖啡渣 Coffee grounds	Some rom CB conductive dopant	Yes	Pyrolysis of cellulose and lignin forms crystalline graphite domains[26, 27]
无烟煤 Anthracite coal	Some from CB dopant	Yes	Pyrolysis forms crystalline graphite domains[20]

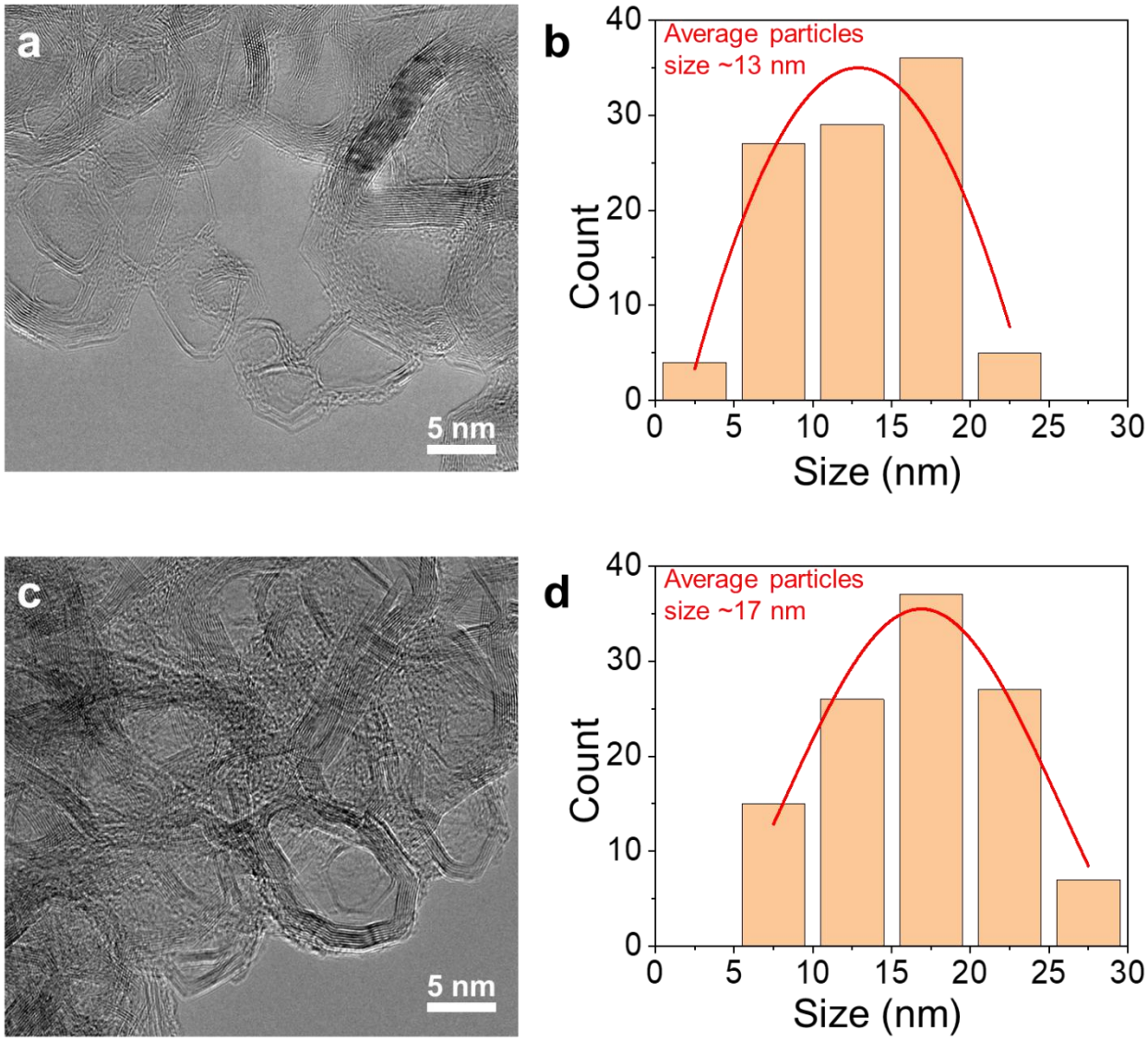

补充图5.CB-FG和CPC-FG的粒度分布. CB的HR-TEM图像-
Supplementary Fig. 5. **Size distribution of CB-FG and CPC-FG.** a. HR-TEM image of CB-
CB-FG尺寸分布直方图. CPC-FG的HR-TEM图像. CPC-FG
FG. b. Histogram for size distribution of CB-FG. c. HR-TEM image of CPC-FG. d. Histogram
粒度分布直方图.
for size distribution of CPC-FG.

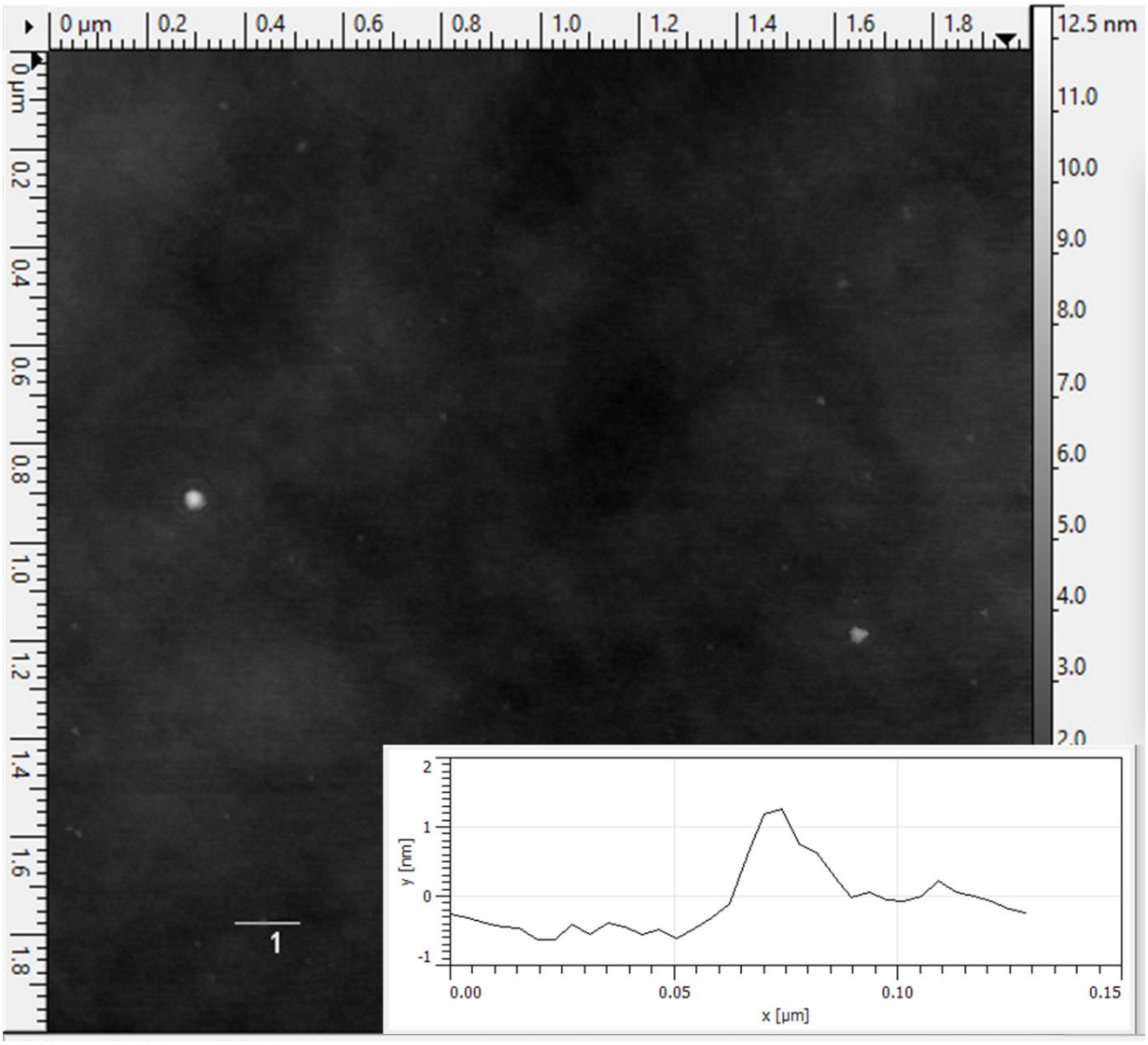

补充图6.炭黑衍生功能梯度的原子力显微镜表征. CB-FG是

Supplementary Fig. 6. **AFM characterization of carbon black-derived FG.** CB-FG is

分散在N-甲基-2-吡咯烷酮(NMP)溶液中并沉积在硅酮基底上.

dispersed in *N*-methyl-2-pyrrolidone (NMP) solution and deposited onto a silicone substrate. The

如补充图5所示, 单个CB-FG颗粒位于FLG产生的约1.2nm高度的表面上.

individual CB-FG particles as seen from Supplementary Fig. 5 lay on the surface with height of

~ 1.2 nm that result from FLG.

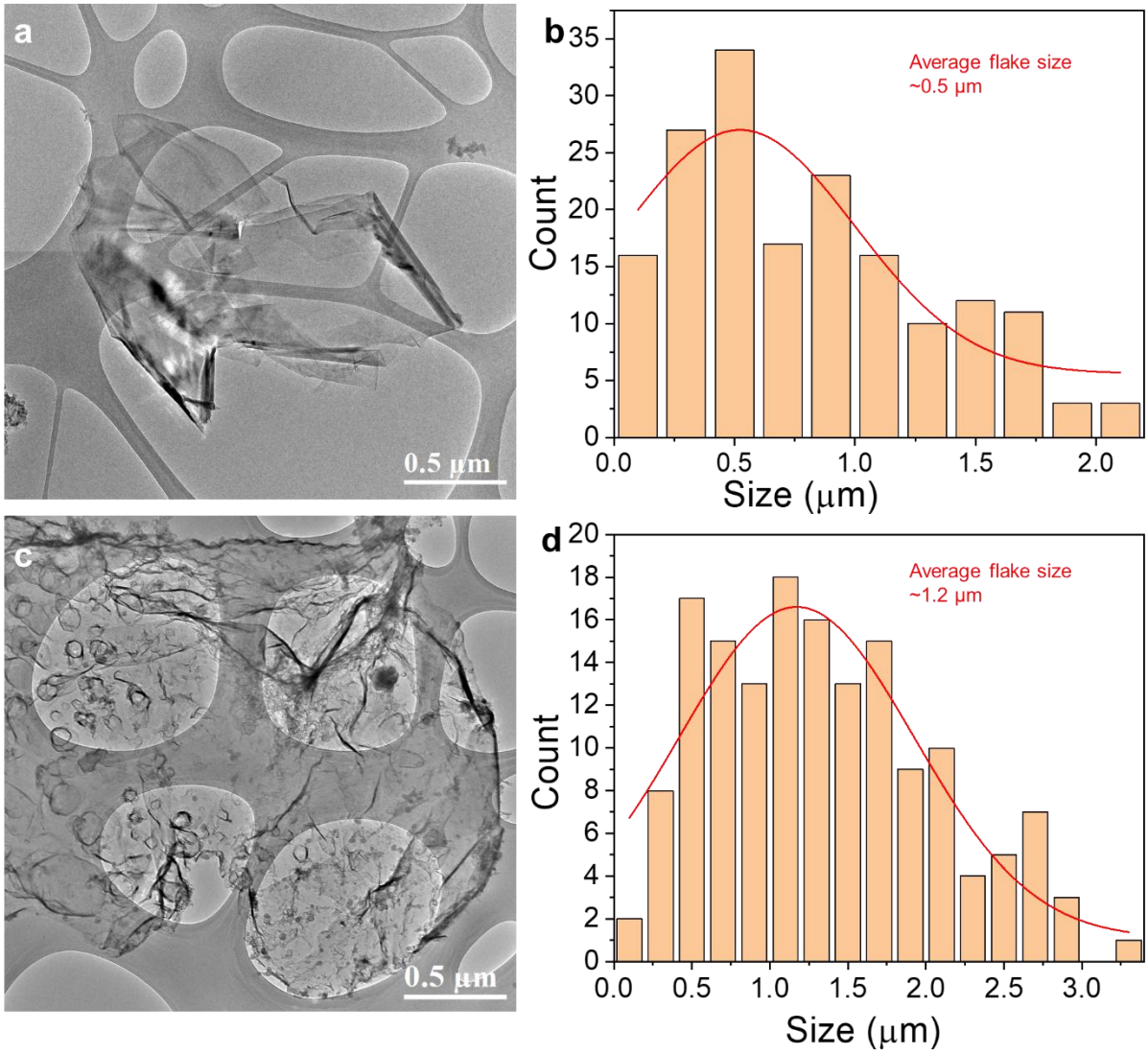

补充图7.无烟煤和咖啡衍生纤维的粒度分布.

Supplementary Fig. 7. Size distribution of anthracite- and coffee-derived FG. a. HR-TEM image of A-FG. b. Histogram for size distribution of A-FG. c. HR-TEM image of C-FG. d. Histogram for size distribution of C-FG.

A-FG图像. A-FG大小分布直方图. C-FG的HR-TEM图像. C-FG大小分布直方图.

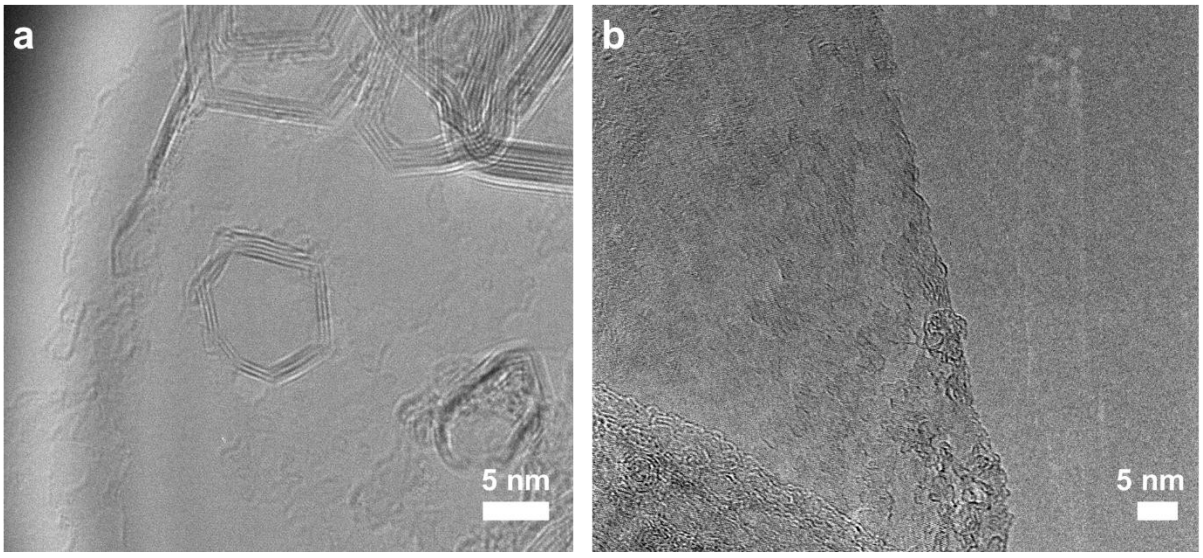

补充图8.(a)C-FG和(b)a-FG单层石墨烯的TEM图像.

Supplementary Fig. 8. TEM images of single layer of graphene from (a) C-FG and (b) A-FG.

CB-FG具有多面体石墨烯,这也可能来自用于提高FJH导电性的CB掺杂剂.

The CB-FG has some polyhedral graphene that could also come from the CB dopant used to increase the conductivity for FJH.

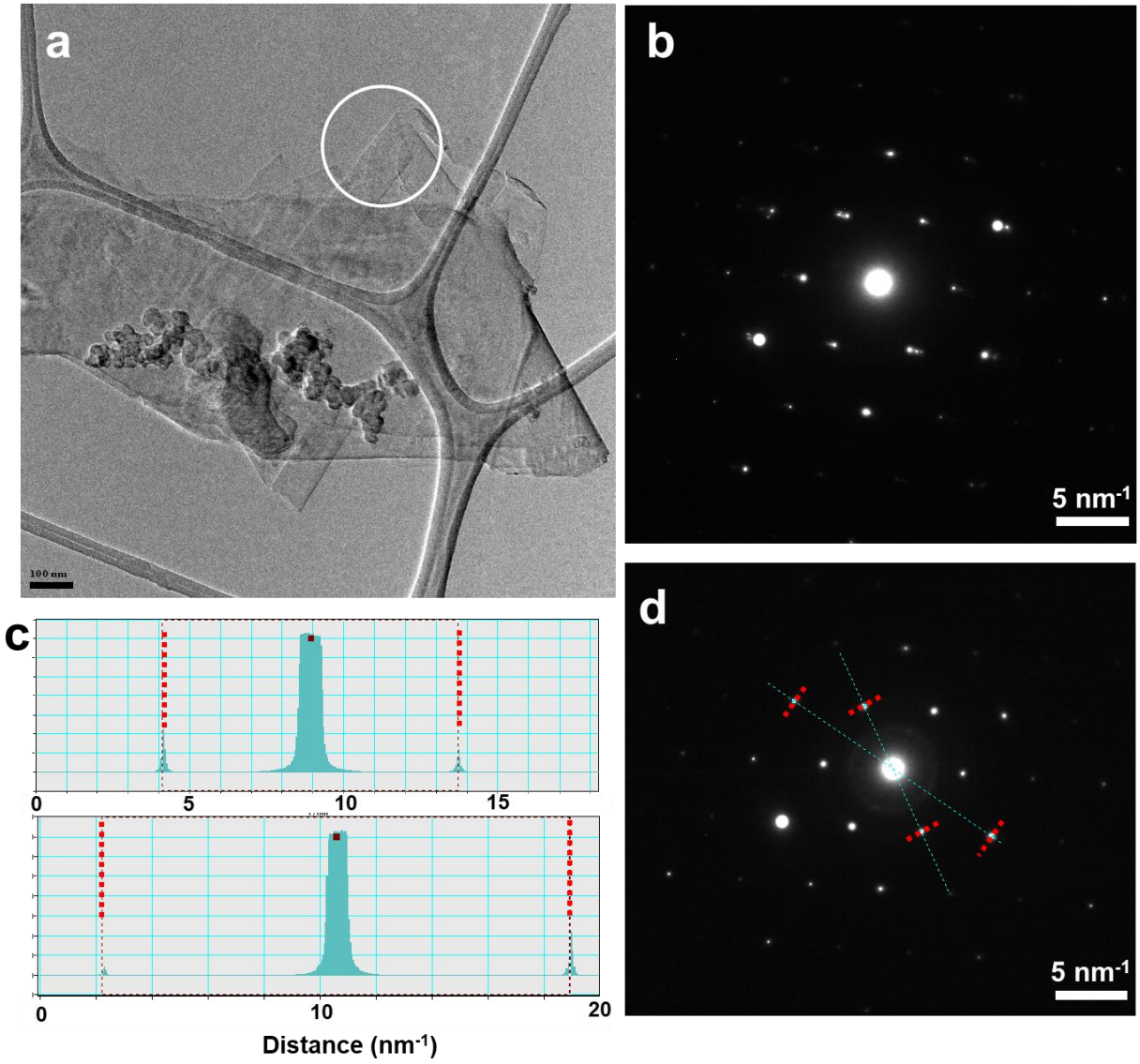

补充图9.无烟煤衍生燃料的SAED. a-FG薄片和
Supplementary Fig. 9. **SAED of anthracite-derived FG**. a. TEM image of a A-FG flake and
SAED的位置. 少数层石墨烯位置的SAED, 显示层之间的不对中.
the position for SAED. b. SAED of the few-layer graphene position that shows misalignment
与SLG相关的SLG的SAED.
between layers. c-d. SAED of SLG that correlates with SLG in previous studies.[28, 29]

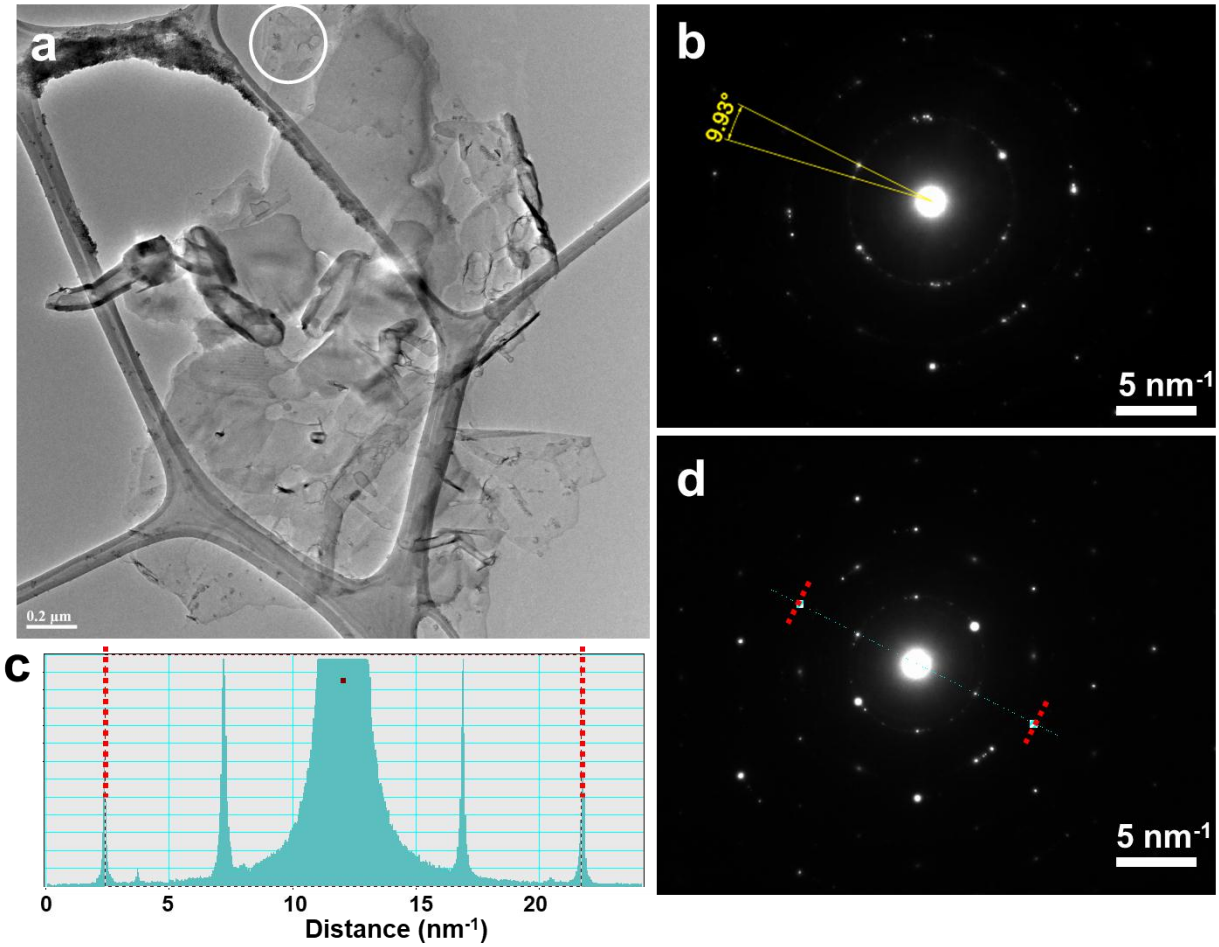

补充图10.咖啡衍生产品的SAED. C-FG薄片的TEM图像和
Supplementary Fig. 10. **SAED of coffee-derived FG**. a. TEM image of a C-FG flake and the
SAED的位置. 少数层石墨烯位置的SAED, 显示层之间的不对中.
position for SAED. b. SAED of the few-layer graphene position that show misalignment
在以前的研究中与SLG相关的SLG的SAED.
between layers. c-d. SAED of a SLG that correlates with SLG in previous studies.[28, 29]

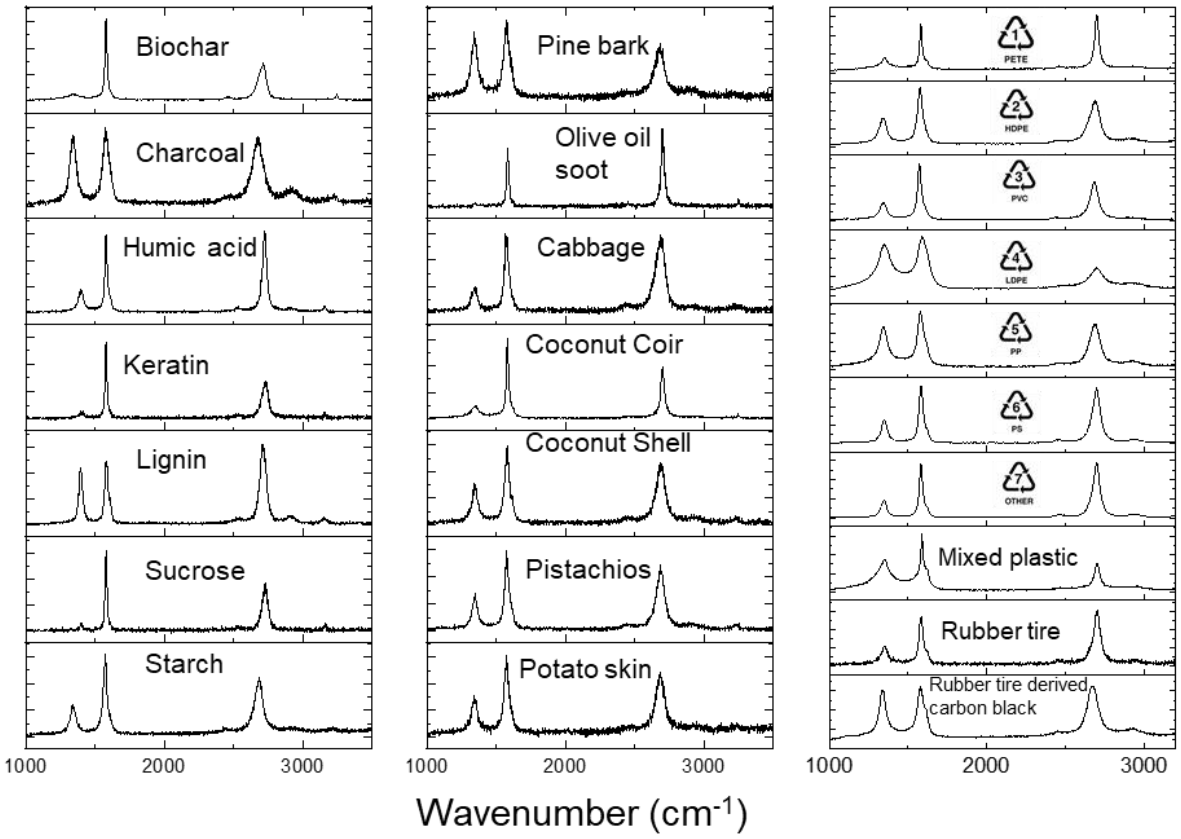

补充图11.其它碳源FG的典型拉曼光谱.

Supplementary Fig. 11. Representative Raman spectra of FG derived from other carbon sources.

这些都没有为FJH条件优化, 以最大限度地提高石墨烯的质量.

None of these have been optimized for FJH conditions to maximize the graphene quality.

生物炭具有足够的导电性, 不需要添加剂. 所有其他非塑料样品都添加了

Biochar was sufficiently conductive; it needed no additive. All other non-plastic samples had 5

5-10 wt%的炭黑以提高其导电性. 所有塑料样品都添加了5 wt%的炭黑以提

to 10 wt% CB added to increase their conductivities. All plastic samples had 5 wt% CB added to

高其导电性. 或2-5 wt%的FG可以用来代替CB作为导电添加剂, 但这些光谱

increase their conductivities. Or 2 to 5 wt% of FG from a previous run can be used to substitute

没有显示在这里. #7塑料, 其他,

the CB as the conductive additive, but those spectra are not shown here. #7 plastic, "OTHER",

是聚丙烯腈(PAN). 混合塑料由以下重量百分比的聚合物制成：HDPE 40%, PETE

is polyacrylonitrile (PAN). Mixed plastic was made from the following wt% of polymers: HDPE

40%, PP 10%, PVC 10%.

40%, PETE 40%, PP 10%, PVC 10%.

补充表4.补充图11的前体源.松树皮、橄榄油烟灰、卷心菜、人发角蛋白、椰子、开心果壳、
Supplementary Table 4. Precursor sources for Supplementary Fig. 11. Pine bark, olive oil soot,
土豆皮、PETE、HDPE、PVC、LDPE、PP、PS等作为废品收集, 不采购.
cabbage, keratin from human hair, coconut, pistachio shells, potato skins, PETE, HDPE, PVC,

LDPE, PP, and PS were collected as waste products, so they were not purchased.

生物炭	Neroval有限责任公司, 来自田纳西州混合区
Biochar 木炭	Neroval LLC, from mixed Tennessee 硬木, 1100 ° C下商业化处理 hardwoods, commercially prepared at 1100°C
Charcoal	Sigma CAS: 7440-44-0
Humic acid	Sigma CAS: 1415-93-6
Lignin	Sigma CAS: 8068-05-1
Sucrose 淀粉	Sigma CAS: 57-50-1 无精蛋白
Starch	Argo gluten free
PAN 橡胶轮胎衍生炭黑.	Sigma CAS: 25014-41-9
Rubber tire-derived carbon black	Ergon Asphalt and Emulsion Inc.

智科眼【https://www.zhisci.com】英文PDF论文，一键免费变中英双语对照！

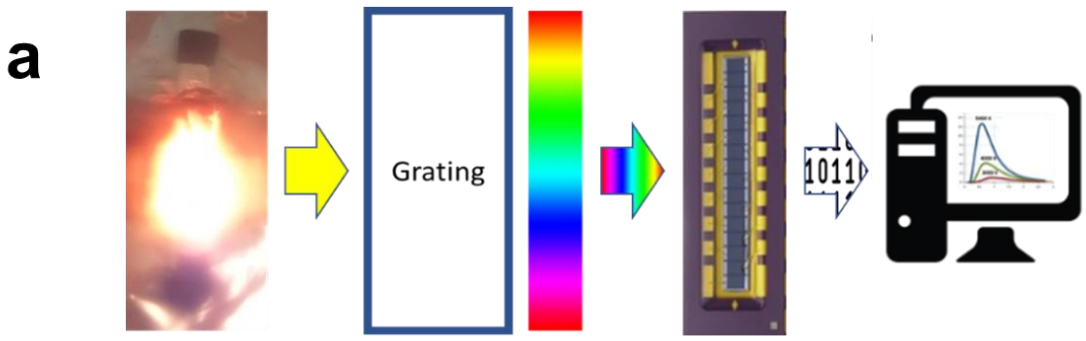

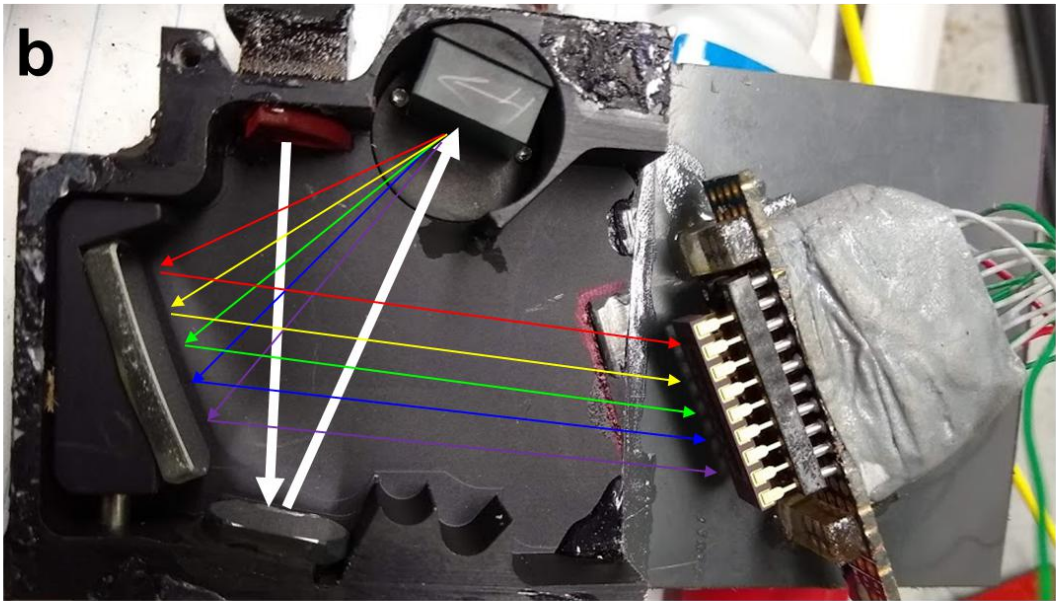

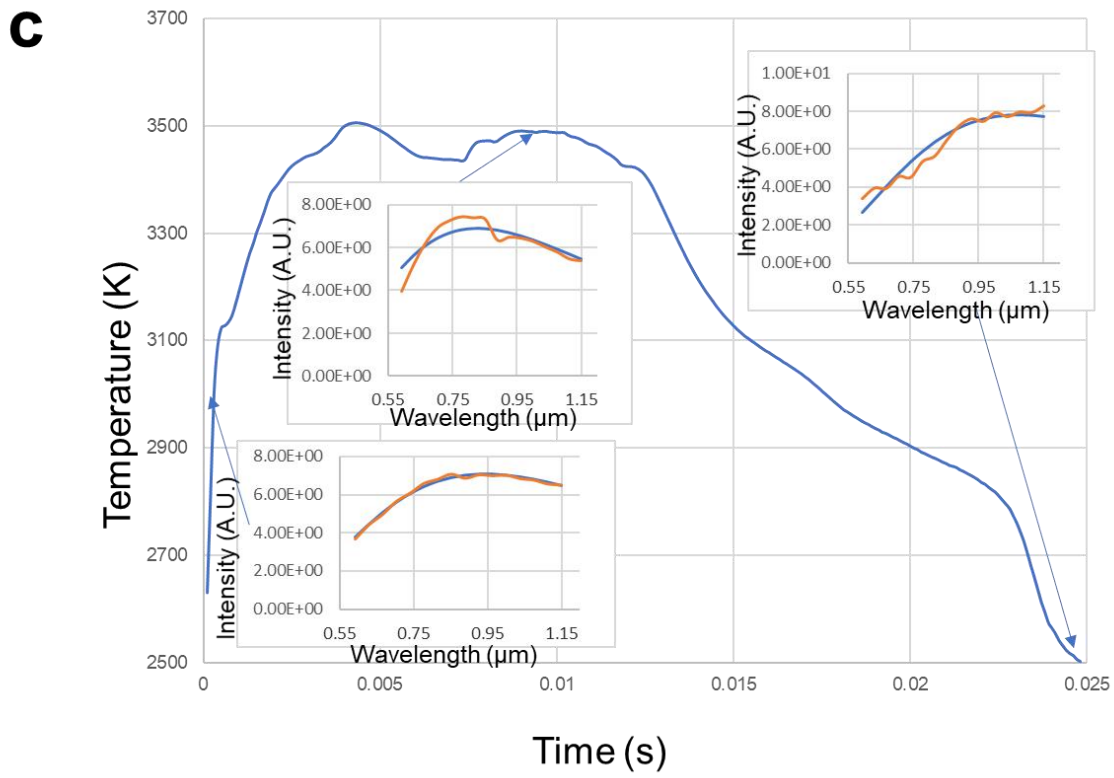

智科眼【https://www.zhisci.com】英文PDF论文，一键免费变中英双语对照！

补充图12.超快速温度测量.自建温度测量装置示意图

Supplementary Fig. 12. Ultrafast temperature measurement. a. Schematic of the home-built temperature measurement set up. b. Black body radiation from the sample is collected by an optical fiber through a customized grating black box. The spectrum of the radiation populates a 16 pixels photodiode arrays (Hamamatsu S4111-16R) at 600 nm to 1100 nm. Light paths are illustrated. The reversed bias voltages (9 V) from the photodiode arrays are collected by the National Instrument multifunction I/O device PCIe-6320. c. Black body radiation fitting. The temperature from each point of the temperature *vs* time graph is determined by the black body radiation fitting of the spectrum from 0.6-1.1 μm emission. Inset is spectrum fitting for 3000 K, 3500 K and 2500 K.

样品中的黑体辐射由光纤通过定制的光栅黑匣子收集.
辐射光谱在600 nm到1100 nm处填充
16像素光电二极管阵列(Hamamatsu S4111-16R).
光路如图所示.
来自光电二极管阵列的反向偏置电压(9v)由国家仪器多功能输入/输出设备PCIe-6320收集.c.
黑体辐射装置.
温度与时间关系图中每个点的温度由0.6-1.1μm发射光谱的黑体辐射拟合确定.
插图是3000 K、3500 K和2500 K的光谱拟合图.

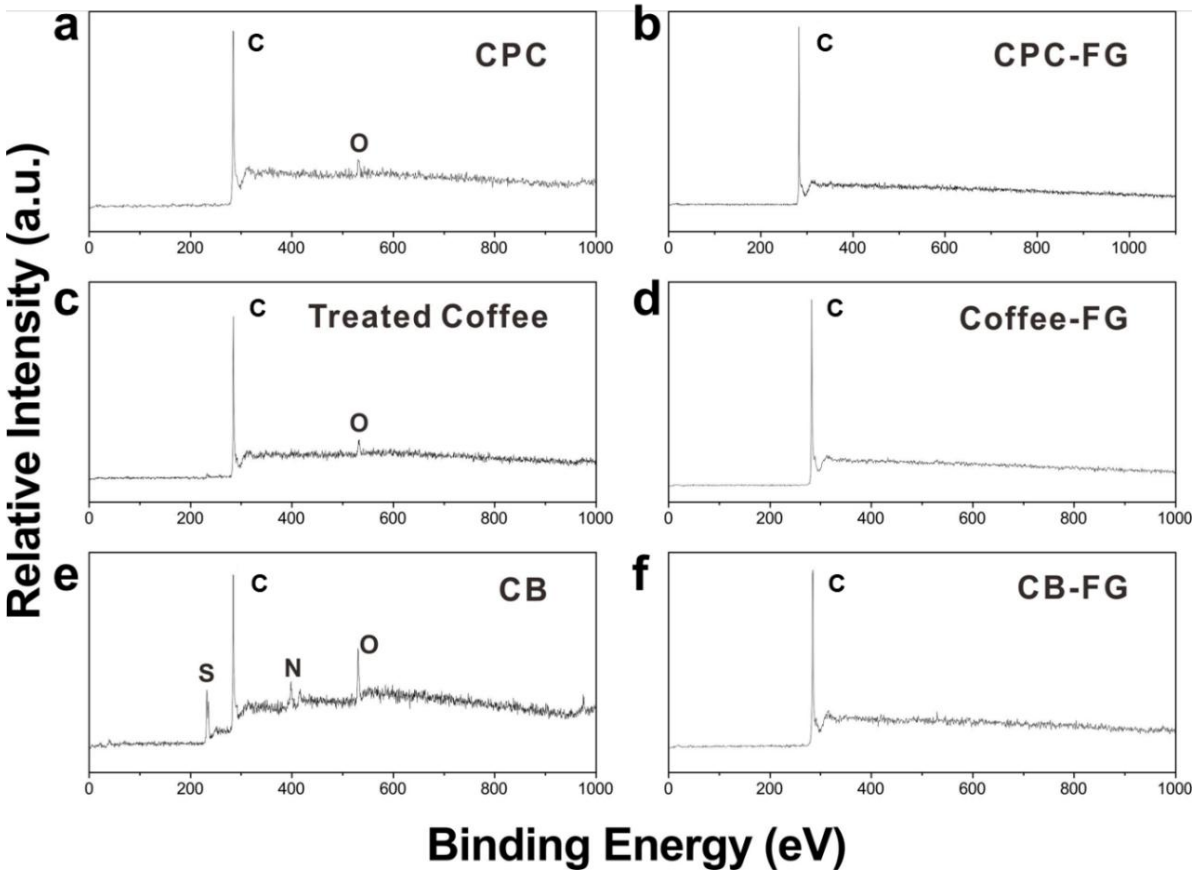

补充图13.煅烧石油焦、预处理(见正文)咖啡渣和炭黑在FJH工艺前后的XPS.

Supplementary Fig. 13. XPS of calcined petroleum coke, pre-treated (see main text) coffee grounds and carbon black before and after the FJH process. Significant reduction in contaminants is seen with FG from carbon black.

炭黑中的FG可以显著减少污染物.

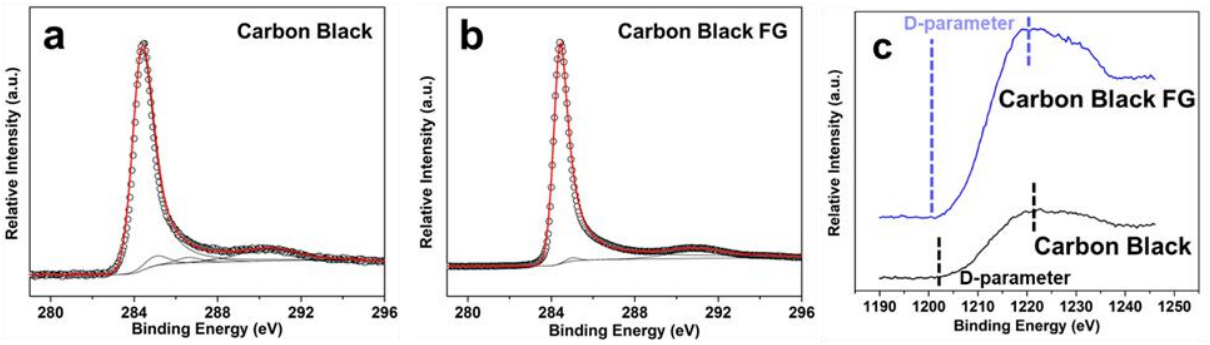

d	C=C (sp2)	C-C (sp3)	C-O/C-O-C	O-C=O/C=O
CB (%)	90.9	4.7	2.8	1.6
CB-FG (%)	98.6	1.4	0	0

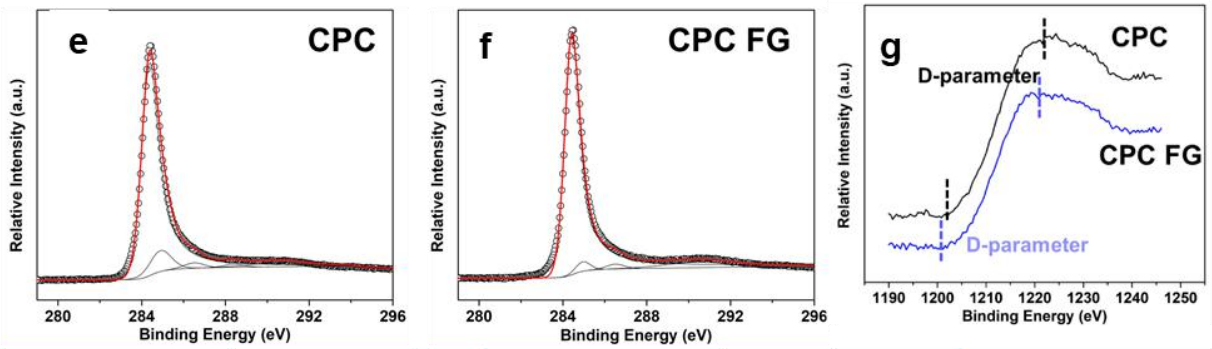

h	C=C (sp2)	C-C (sp3)	C-O/C-O-C	O-C=O/C=O
CPC (%)	84.7	11.1	2.6	1.5
CPC-FG (%)	93.9	3.7	2.4	0

补充图14.CB-FG和CPC C 1s光谱的高分辨XPS研究-

Supplementary Fig. 14. High resolution XPS of the C 1s spectrum from CB-FG and CPC-

CB和CB-FG的C-KLL光谱的高分辨率X射线光电子能谱. D参

FG. a. CB. b. CB-FG. c. High resolution XPS of C KLL spectrum of CB and CB-FG. The D-

数测量了区分C-KLL谱中最大值和最小值之间的能量分离.

parameter measures the energy separation between maxima and minima in differentiated C KLL

在金刚石和石墨烯中, 其值分别为13ev和21ev. 值越大,

spectra. In diamond and graphene, the values are 13 eV and 21 eV, respectively. The larger

表示sp2/sp3比值越高. 30对于CB和CB-FG, 数值分别为20.5 eV和20.9 eV.

values infer a higher sp^2/sp^3 ratio.[30] For the CB and CB-FG, the values are 20.5 eV and 20.9 eV,

因此, FJH工艺后, 从CB到CB-FG的sp2/sp3比值增加.

respectively. Thus, after the FJH process, the sp^2/sp^3 ratio increases in going from CB to CB-FG.

CB和CB-FG的反卷积C 1s峰高分辨谱的相对分布.
d. Relative distribution of deconvoluted C 1s peak high resolution spectrum of CB and CB-FG.
sp2碳(C=C)的相对分布由90.9%增加到98.6%, sp3碳(C-
Relative distribution of sp^2-carbon (C=C) increases from 90.9% to 98.6% and the sp^3-carbon (C-
C) 从4.7%降至1.4%. 因此, 经过FJH处理后, sp2/sp3比值增大, 与
C) decreases from 4.7 % to 1.4 %. Thus, the sp^2/sp^3 ratio increases after the FJH process,
CB-FG拉曼光谱中的极高2D/G比值发生腐蚀. CPC和
corroberating with the very high 2D/G ratio in the Raman spectra of CB-FG. d. Relative
CPC-FG的反卷积C 1s峰高分辨谱的相对分布.
distribution of deconvoluted C 1s peak high resolution spectrum of CPC and CPC-FG. The
FJH工艺后, sp2/sp3比值从7.6增加到25.2, 这与
sp^2/sp^3 ratio increases from 7.6 to 25.2 after the FJH process, corroborating with the very high
CPC-FG拉曼光谱中的2D/G比值.
2D/G ratio in the Raman spectra of the CPC-FG.

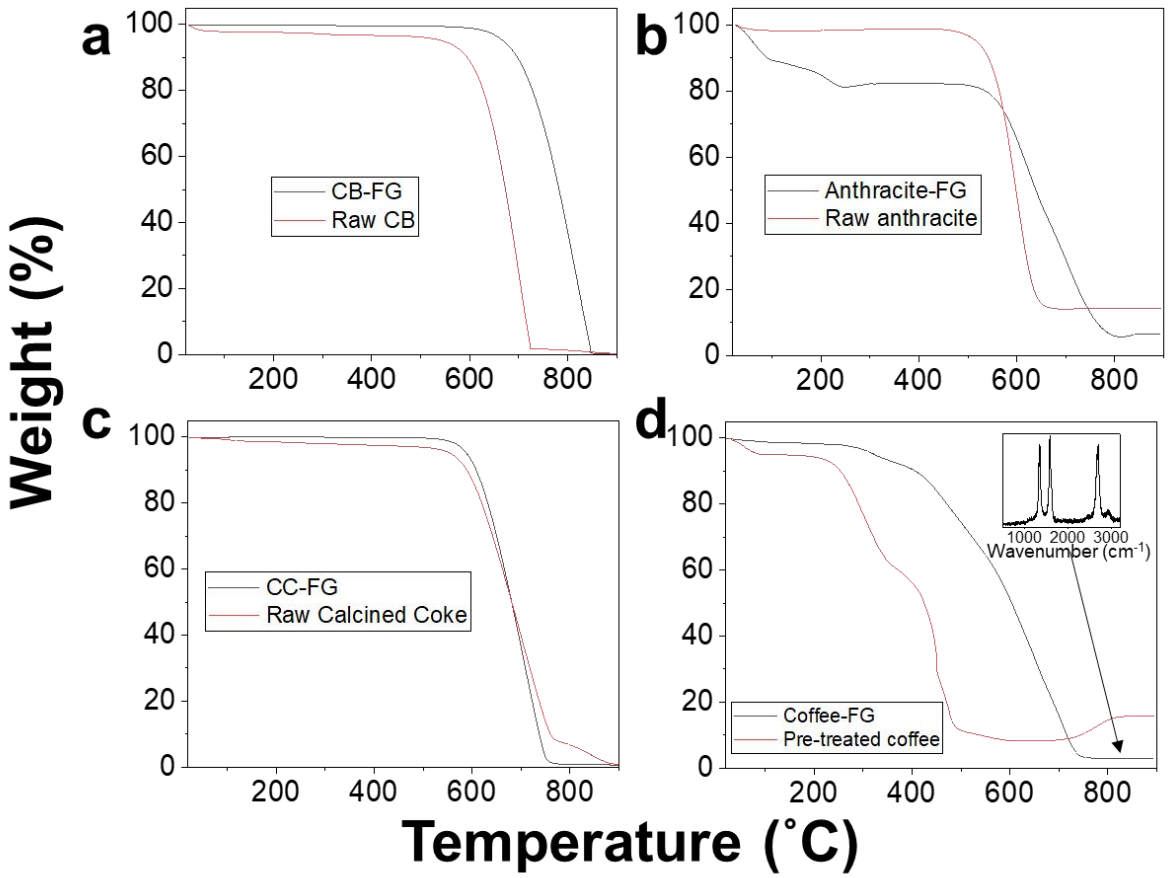

补充图15.空气中热重分析：a. 生CB(黑珍珠2000, 卡博特)和CB-FG.
Supplementary Fig. 15. TGA in air of: a. Raw CB (Black Pearls 2000, Cabot) and CB-FG. b.
无烟煤和无烟煤原料. 生焦和CC-FG. 预处理咖啡
Raw anthracite coal and anthracite-FG. c. Raw calcined coke and CC-FG. d. Pre-treated coffee

还有咖啡-FG. 在炭黑、无烟煤和咖啡中,前驱体材料和衍生FG之间的最终重量显著降低.
and coffee-FG. With carbon black, anthracite coal and coffee, there is significant decrease in the
对TGA残渣的XPS分析表明,
final weight between the precursor material and the derived FG. XPS of the TGA residue shows
无烟煤FG的TGA残渣中含有C(15%)、O 62%、Si(11%)和Al(12.6%);咖啡FG的TGA残渣中含有
that the TGA-residue from anthracite-FG contains of C (15%), O 62 %, Si (11%) and Al (12.6%);
C(65%)、O(25%)、S(2.9%)和P(2%). 此外,用
and residue from coffee-FG contains of C (65%), O (25%), S (2.9%) and P (2%). Furthermore,
拉曼光谱(插图d)分析了咖啡纤维蛋白g中的TGA残基,结果表明它是显著的石墨烯.
the TGA-residue from coffee-FG was analyzed by Raman spectroscopy (inset in d) to show that

it is significantly graphene.

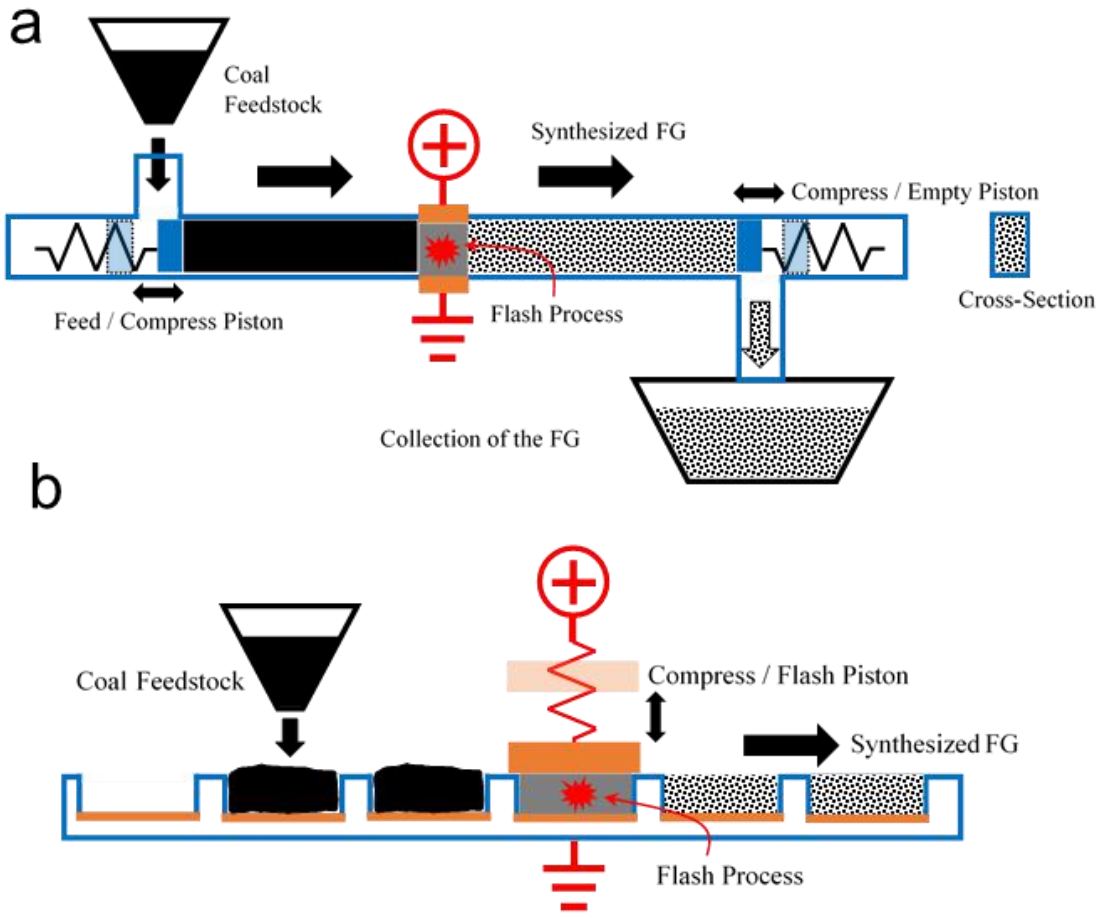

补充图16.用于FG过程自动化的可能反应器, 例如煤源.
Supplementary Fig. 16. Possible reactors for automation of the FG process, for example with a
连续活塞成形工艺. 与实验室的设置不同, 压缩活塞和电极的功
coal source. a. Continuous piston FG process. Unlike the laboratory setup, the function of the
能是由单独的部件执行的. 合适
compression pistons and the electrodes is carried out by separate components. Suitable
的电极是铜、不锈钢、石墨或钨电极, 它们附着在石英上, 但有排气孔, 以便在FJH过
electrodes are copper, stainless steel, graphite or tungsten electrodes that are attached to the
程中排出热的工艺气体.
quartz but have vent holes to enable escape of the hot process gases during the FJH process. The
压缩活塞可以由介电材料制成, 可能是石英或陶瓷, 以防止对活塞接地短路.
compression pistons can be made of a dielectric material, possibly quartz or ceramic, to prevent
在这个连续的过程中, 碳原料通过一个储液罐进入过程管
shorting to the piston's ground. In this continuous process, carbon feedstock is fed through a
(借助于振动筛), 同时压缩活塞缩回左侧.
reservoir into the process tube (aided by a shaker) while the compression piston is retracted to
在管内分配碳粉后, 进料压缩活塞以足够的行程移动, 以从电极下方(JH区域)置换转
the left. After the carbon powder is dispensed in the tube, the Feed Compress Piston moves with
换的碳, 同时空压缩活塞向右缩回, 以允许将FG排空到收集仓(借助振动筛或真空吸力).
enough stroke to displace the converted carbon from underneath the electrodes (JH region) while

at the same time the Empty Compress Piston retracts to the right to allow FG to be emptied into a
闪光结束后, 空活塞推动堵塞管道,
collection bin (aided by a shaker or a vacuum suction). After the strike is over, the Empty Piston
而进料活塞对煤施加预定压力, 直到FJH工艺完成.
pushes in to block the tube while the Feed Piston applies predetermined pressure to the coal until
活塞循环需要与连续过程的生产量相匹配.
the FJH process is done. The piston cycles need to match the throughput of the continuous
碳纤维/FG材料的流动是在一个封闭的环境中, 使操作安全.
process. The flow of carbon/FG material is in an enclosed environment that makes the operation
连续输送带FG工艺. 在该反应中, 煤原料通过储层被送入石英或陶瓷舟中,
safe. b. Continuous Belt FG Process. In this reaction, the coal feedstock is fed through a reservoir
该石英或陶瓷舟具有电接地的金属底部电极, 并且是连续带的一部分.
into the quartz or ceramic boat, having a metallic bottom electrode that is grounded electrically,

and is part of a continuous belt.

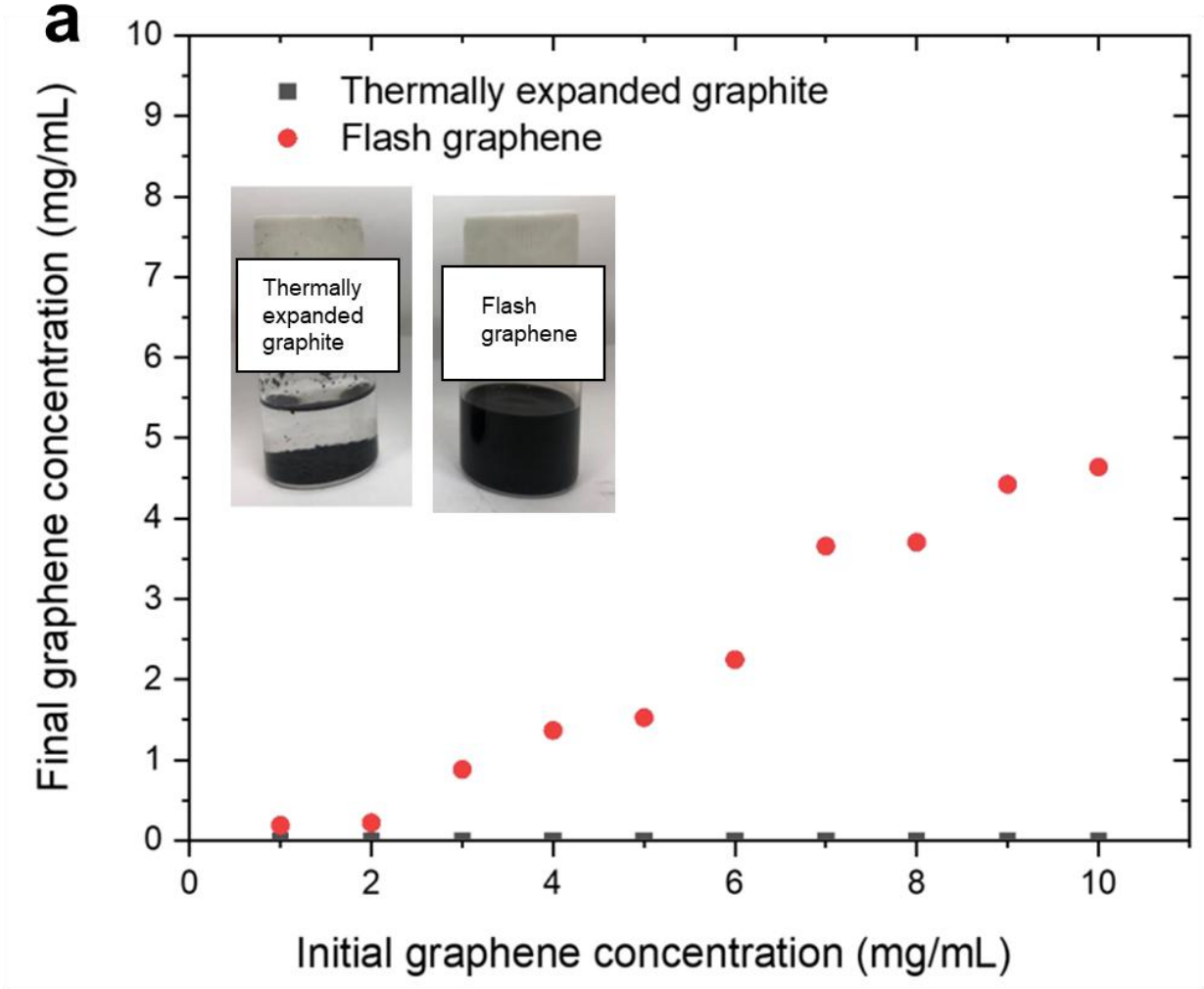

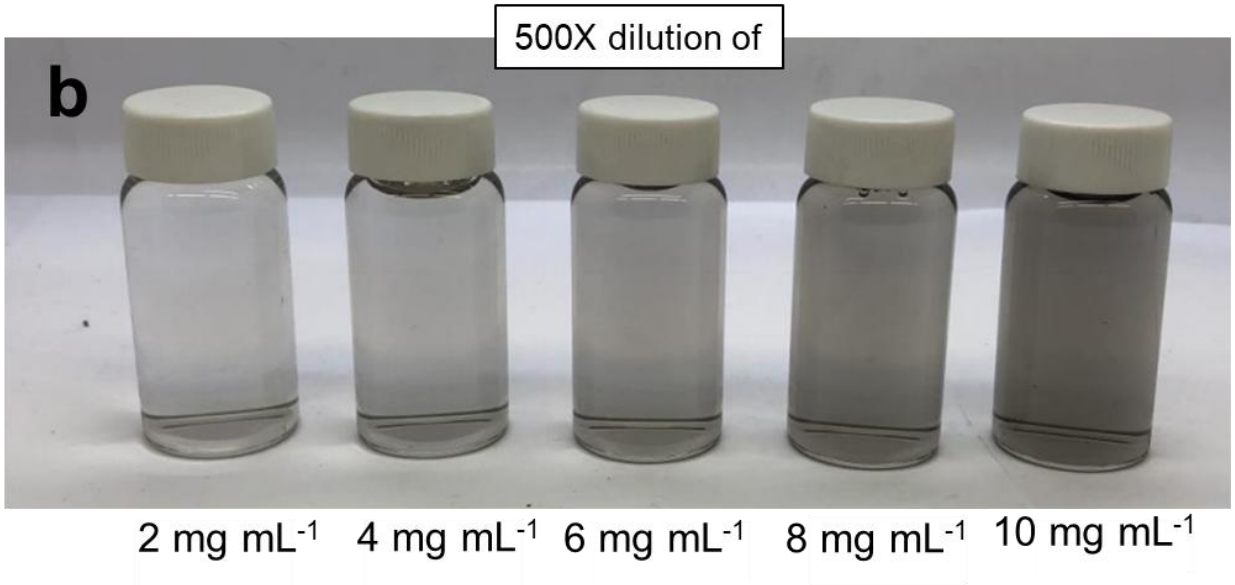

智科眼【https://www.zhisci.com】英文PDF论文，一键免费变中英双语对照！

补充图17.FG在水中的分散性/Pluronic(F-127)(1%). 5mg mL-1热
Supplementary Fig. 17. FG dispersion in water/Pluronic (F-127) (1%). a. Comparison of
膨胀石墨与CB-FG在水/Pluronic(F-127)(1%)中的分散性比较.
dispersibility of 5 mg mL^{-1} of thermally expanded graphite and CB-FG in water/Pluronic (F-127)
热膨胀石墨在离心后沉降(见方法), 而CB-FG仍分散在水表面活性剂溶液中.
(1%). The thermally expanded graphite settles after centrifugation (see Methods) while the CB-
CB-FG的视觉分散性.
FG remains dispersed in the water surfactant solution. b. Visual dispersibility of CB-FG. The
原始浓度在图像下方指定, 但该浓度被稀释500倍, 以直观显示CB-FG的分散性.
original concentration is specified below the image but that concentration was diluted 500x for
在所有稀释溶液中均未发现肉眼可见的大颗粒.
visual demonstration of CB-FG dispersibility. No large particles are found visually in all diluted
solutions.

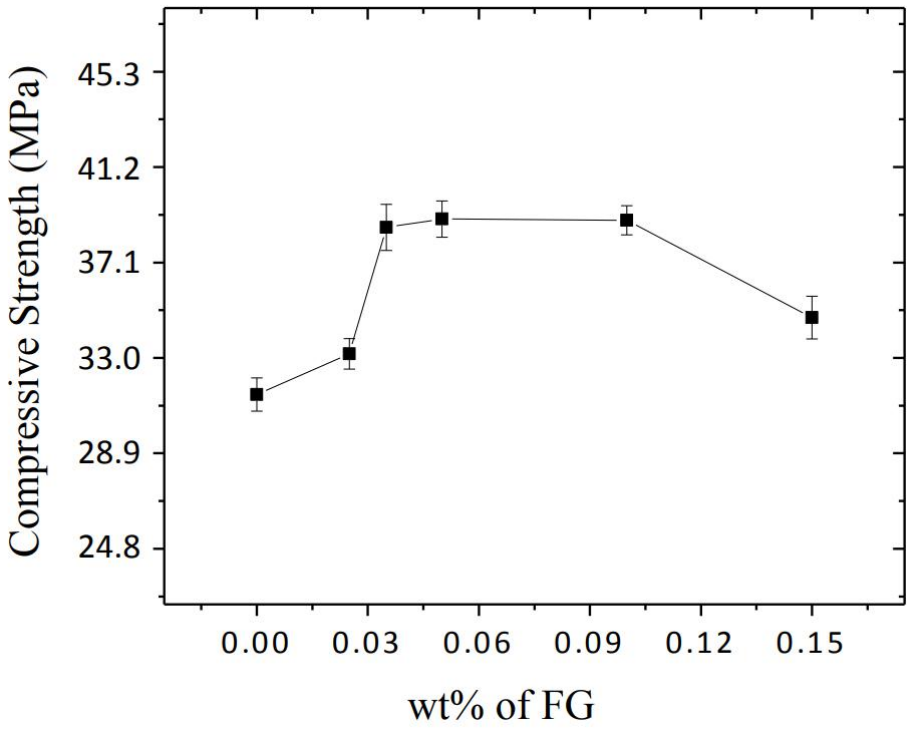

补充图18.CB-FG/水泥复合材料的力学性能
Supplementary Fig. 18. Mechanical properties of the CB-FG/cement composites measured at
28天.
28 days.

智科眼【https://www.zhisci.com】英文PDF论文，一键免费变中英双语对照！

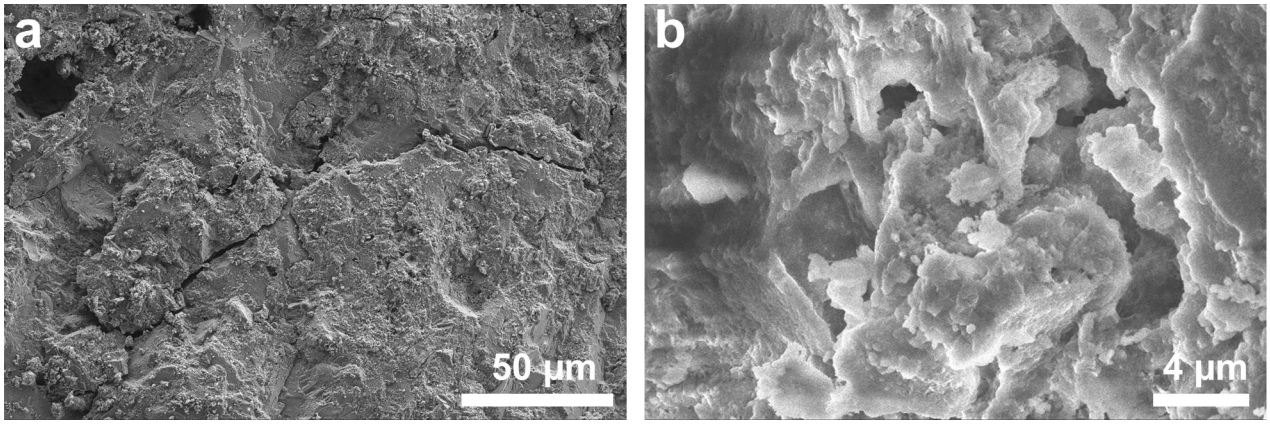

补充图19.水泥与CB-FG复合材料的SEM图像. 扫描电镜照片显示石

Supplementary Fig. 19. SEM images of cement and CB-FG composite. The SEM images show

墨烯在硅酸盐水泥中分散良好, 没有明显的石墨烯大薄片.

good graphene dispersion in Portland cement without any visible large flakes of graphene.

CB-FG/水泥复合材料性能的大幅度提高可能是由于涡轮层CB-FG在水中易于分散, 均匀分布的

The large enhancement in the properties of CB-FG/cement composites could be due to the ease

片状FG作为模板促进水泥水化产物的均匀生长.

of dispersibility of the turbostratic CB-FG in water where the homogenously distributed sheet-

like FG acts as templates to promote congruent growth of cement hydrate products.[31]

此外, 有文献表明, 石墨烯和水泥水合物之间的共价C-O键/网络可以在共价键形成时改变

Additionally, there is literature suggestion that covalent C-O bonds/networks between graphene

石墨烯从sp2到sp3的杂化, 大大提高复合材料的力学性能, 尽管我们无法验证或证实该

and cement hydrate products can change the hybridization of graphene from sp^2 to sp^3 upon

反应的机理.

covalent bond formation, greatly enhancing the mechanical properties of the composite, though

有人认为, 这种变化以及

we cannot verify or substantiate the mechanism for that reaction.[32] It has been suggested that this

界面附近的电子释放, 可导致性能改善的均匀、混合和插层复合材料.

change, along with electron release in the vicinity of their interfacial region, can lead to

这是否发生

homogenous, inter-mixed and intercalated composites with improved properties. Whether this is

在这里还没有实验证实.

taking place here has not been experimentally verified.

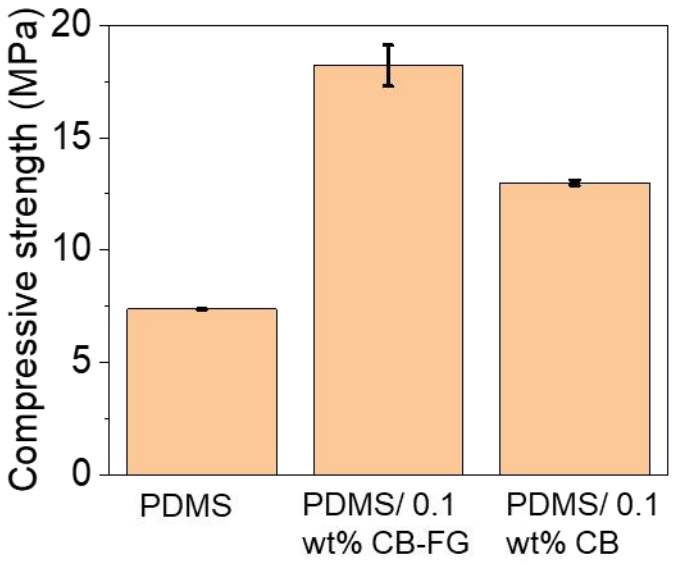

补充图20.PDMS、CB-FG/PDMS复合材料和
Supplementary Fig. 20. Compressive strength of PDMS, CB-FG/PDMS composite and
CB/PDMS复合材料.
CB/PDMS composite.

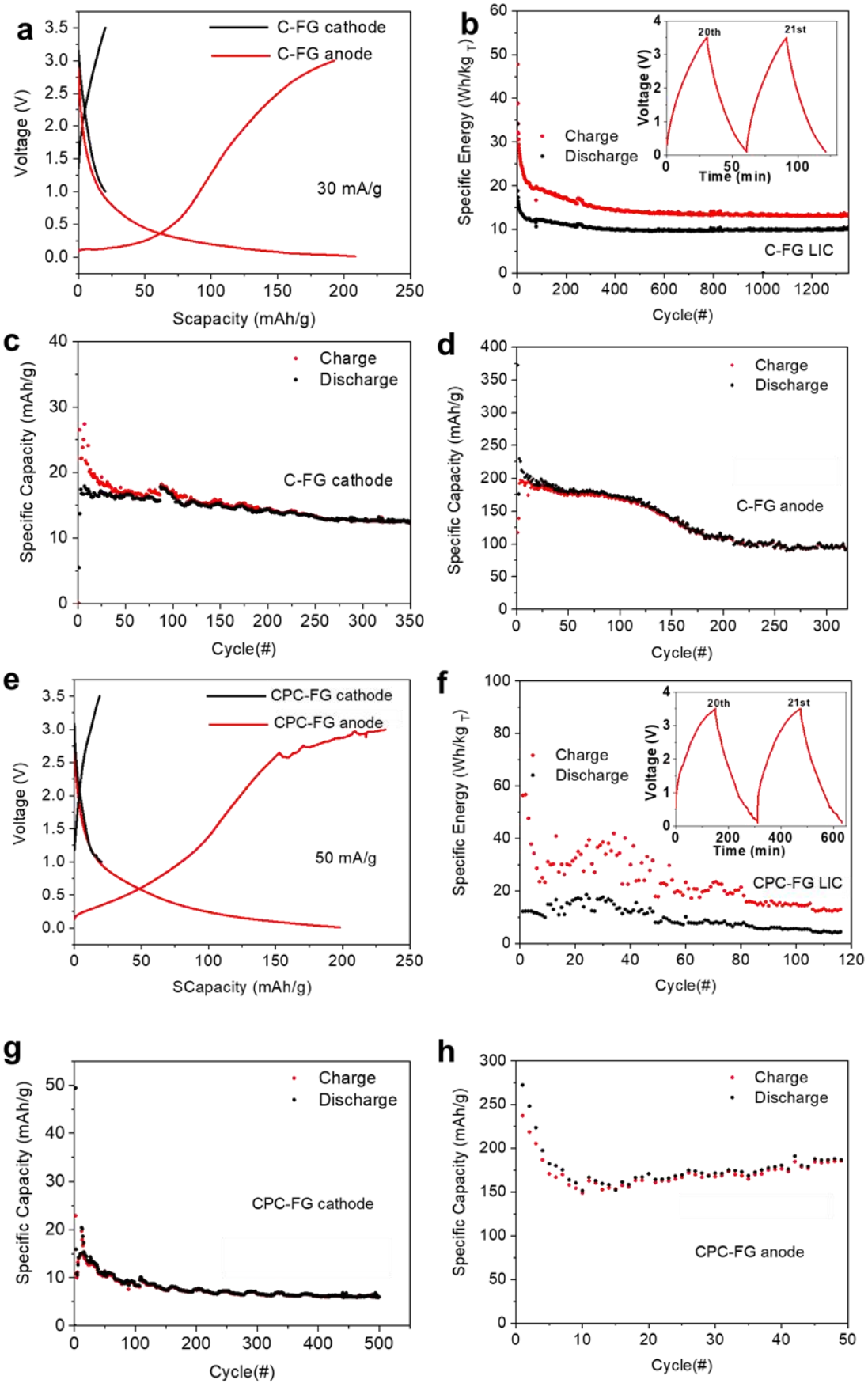
a
C-FG cathode
C-FG anode
30 mA/g
Voltage (V)
Scapacity (mAh/g)
b
Charge
Discharge
20th
21st
Voltage (V)
Time (min)
Specific Energy (Wh/kg T)
C-FG LIC
Cycle(#)
c
Charge
Discharge
C-FG cathode
Specific Capacity (mAh/g)
Cycle(#)
d
Charge
Discharge
C-FG anode
Specific Capacity (mAh/g)
Cycle(#)
e
CPC-FG cathode
CPC-FG anode
50 mA/g
Voltage (V)
SCapacity (mAh/g)
f
Charge
Discharge
20th
21st
Voltage (V)
Time (min)
Specific Energy (Wh/kg T)
CPC-FG LIC
Cycle(#)
g
Charge
Discharge
CPC-FG cathode
Specific Capacity (mAh/g)
Cycle(#)
h
Charge
Discharge
CPC-FG anode
Specific Capacity (mAh/g)
Cycle(#)

补充图21.在锂离子电容器和锂离子电池中. 制作并循环使用锂
Supplementary Fig. 21. FG in a Li-ion capacitor and a Li-ion battery. A Li-ion battery was
离子电池, 打开电池, 用阳极和阴极制作锂离子电容器.
made and cycled, then the battery was opened and the anode and cathode were used to make the
C-FG阳极(0.01-3.0v)和阴极(13.5v)的锂离子电池的充放电曲线.
Li-ion capacitor. a. Charge/discharge curves of the Li-ion battery with C-FG anodes (0.01−3.0 V)

and cathodes (1−3.5 V) in half-cells with Li foil as the counter and reference electrode. b. Long-
C-FG锂离子电容器在20ma.g-1下的长程稳定性.c. C-FG阴极半电池在30ma.g-1下的
range stability of C-FG Li-ion capacitor at 20 mA.g^{-1}. c. Cycling performance of the Li-ion
循环性能.d. 以C-FG为阳极半电池的锂离子电
battery with the C-FG cathode half-cell at 30 mA.g^{-1}. d. Cycling performance of the Li-ion
池在50ma.g-1下的循环性能.e.以锂箔为计数电极和参比电极的半电池中煅烧石油焦
battery with C-FG as the anode half-cell at 50 mA.g^{-1}. e. Charge/discharge curves of the Li-ion
FG(CPC-FG)阳极(0.013.0v)和阴极(13.5v)锂离子电池的充放电曲线.
battery with calcined petroleum coke-FG (CPC-FG) anode (0.01−3.0 V) and cathode (1−3.5 V)
CPC-FG锂离子电容器在
in half-cells with Li foil as the counter and reference electrode. f. Long-range stability of the
5mA.g-1下的长程稳定性.g.以CPC-FG为阴极的25ma.g-1锂离子电池的循环性能.h.
CPC-FG Li-ion capacitor at 5 mA.g^{-1}. g. Cycling performance of the Li-ion battery with CPC-
以CPC-FG为阳极半电池的锂离子电池在100ma.g-1下的循环性
FG as cathode at 25 mA.g^{-1}. h. Cycling performance of the Li-ion battery with CPC-FG as the
能.
anode half-cell at 100 mA.g^{-1}.

电化学测试规程
Electrochemical Test Protocols
在CR2032电池上测试了闪蒸石墨烯的电化学性能. 所有电解池
The electrochemical performance of flashed graphene was tested in CR2032 cells. All the cells
均在氩气氛下组装在手套箱中. CR2032锂离子电池由锂箔作对电极,
were assembled in a glove box under argon atmosphere. The CR2032 lithium-ion cell consists of
Celgard K2045作隔膜, 1 M六氟磷酸锂(LiPF6)溶于1:1:1碳酸乙烯酯：碳酸
lithium foil as the counter electrode, Celgard K2045 as the separator, 1 M lithium
二甲酯：碳酸二乙酯(EC:DMC:DEC)(MTI公司)作电解液
hexafluorphosphate (LiPF6) dissolved in 1:1:1 ethylene
, FG(C-FG和CC-FG)作阴极/阳极组成.
carbonate:dimethylcarbonate:diethylcarbonate (EC:DMC:DEC) (MTI corporation) as the
以铝/铜箔为基体, 在N-甲基-2-
electrolyte, and FG (C-FG and CC-FG) as cathode/anode. The cathode/anode were prepared by
吡咯烷酮(NMP)中加入80%活性物质、10%聚偏二氟乙烯(PVDF；Alfa-Aesar)和10%聚偏二氟乙烯
casting slurry which consists 80 wt% active material, 10 wt% (Super P, TIMCAL) and 10 wt%
(TIMCAL).
polyvinylidene difluoride (PVDF; Alfa Aesar) in *N*-methyl-2-pyrrolidone (NMP) on a piece of
在0.01至3.0V的电压范围内进行恒流放电/充电试验
Al/Cu foil. The galvanostatic discharge/charge tests were carried out in voltage range of 0.01 to

智科眼【https://www.zhisci.com】英文PDF论文，一键免费变中英双语对照！

阳极为3.0v(vs Li+/Li), 阴极为1.0～3.5v(vs Li+/Li). 在
3.0 V (vs Li+/Li) for anode and 1.0 to 3.5 V (vs Li+/Li) for cathode, respectively. The full
CR2032电池上测试了锂离子电容器中闪蒸石墨烯的全电容性能.
capacitor performance of flashed graphene in the Li-ion capacitor was tested in CR2032 cells. In
为了组装FG型锂离子电容器, 对锂离子电池半电池的正负极进行了多次循环, 阳极处于放电
order to assemble the FG Li-ion capacitor, the anode and cathode of the Li-ion battery half-cells
状态, 阴极处于充电状态.
were cycled several times with the anode rested at the discharge state and cathode rested at the
两个电池在手套箱中打开, 重新组装成FG锂离子电容器, 在0.1-3.5v电
charge state. The two cells were opened inside a glovebox, re-assembled as a FG Li-ion
压范围内测试. 根据锂离子电池正负极的总质量计
capacitor, and tested in the voltage range of 0.1 to 3.5 V. The capacity of Li-ion capacitor was
算了锂离子电容器的容量.
calculated based on the total mass of the anode plus cathode that had come from the Li-ion
battery.

References

1 Novoselov, K. S. *et al.* Electric field effect in atomically thin carbon films. *Science* **306**, 666-669 (2004).

2 Allen, M. J. *et al.* Honeycomb carbon: a review of graphene. *Chem. Rev.* **110**, 132-145 (2009).

3 Partoens, B. & Peeters, F. M. From graphene to graphite: Electronic structure around the K point. *Phys. Rev. B* **74**, 075404 (2006).

4 Malard, L. M. *et al.* Raman spectroscopy in graphene. *Phys. Rep.* **473**, 51-87 (2009).

5 Bianco, A. *et al.* All in the graphene family – A recommended nomenclature for two-dimensional carbon materials. *Carbon* **65**, 1-6 (2013).

6 Yan, Z. *et al.* Hexagonal graphene onion rings. *J. Am. Chem. Soc.* **135**, 10755-10762 (2013).

7 Kim, K. *et al.* Raman spectroscopy study of rotated double-layer graphene: misorientation-angle dependence of electronic structure. *Phys. Rev. Lett.* **108**, 246103 (2012).

8 Kato, H. *et al.* Growth and Raman spectroscopy of thickness-controlled rotationally faulted multilayer graphene. *Carbon* **141**, 76-82 (2019).

9 Niilisk, A. *et al.* Raman characterization of stacking in multi-layer graphene grown on Ni. *Carbon* **98**, 658-665 (2016).

10 Kiselov, V. *et al.* The growth of weakly coupled graphene sheets from silicon carbide powder. *Semicond. Phys., Quantum Electron. Optoelectron.* 301-307 (2014).

11 Garlow, J. A. *et al.* Large-area growth of turbostratic graphene on Ni (111) via physical vapor deposition. *Sci. Rep.* **6**, 19804 (2016).

12 Ferrari, A. C. *et al.* Raman spectrum of graphene and graphene layers. *Phys. Rev. Lett.* **97**, 187401 (2006).

13 Novoselov, K. S. *et al.*Two-dimensional gas of massless Dirac fermions in graphene. *Nature* **438**, 197 (2005).

14 Ferrari, A. C. Raman spectroscopy of graphene and graphite: Disorder, electron–phonon coupling, doping and nonadiabatic effects. *Solid State Commun.* **143**, 47-57 (2007).

15 Kudin, K. N. *et al.* Raman spectra of graphite oxide and functionalized graphene sheets. *Nano Lett.* **8**, 36-41 (2008).

16 Ni, Z. H. *et al.* Probing Charged Impurities in Suspended Graphene Using Raman Spectroscopy. *ACS Nano* **3**, 569-574 (2009).

17 Ferrari, A. C. & Basko, D. M. Raman spectroscopy as a versatile tool for studying the properties of graphene. *Nat. Nano.* **8**, 235 (2013).

18 Kumar, N. *et al.* High-temperature phase transformation and low friction behaviour in highly disordered turbostratic graphite. *J. Phys. D: Appl. Phys.* **46**, 395305 (2013).

19. Yan, Zheng *et al.* Toward the Synthesis of Wafer-Scale Single-Crystal Graphene on Copper Foils. *ACS Nano* **6**, 9110-9117 (2012).

20. Franklin, R. E. Crystallite growth in graphitizing and non-graphitizing carbons. *Proc. R. Soc. Lond. A.* **209**, 196-218 (1951).

21. Harris, P. J. F. & Tsang, S. C. High-resolution electron microscopy studies of non-graphitizing carbons. *Philos. Mag. A* **76**, 667-677 (1997).

22. Iijima, S. Direct observation of the tetrahedral bonding in graphitized carbon black by high resolution electron microscopy. *J. Cryst. Growth* **50**, 675-683 (1980).

23. Huang, J. Y. *et al.* Real-time observation of tubule formation from amorphous carbon nanowires under high-bias Joule heating. *Nano Lett.* **6**, 1699-1705 (2006).

24. Wang, B. *et al.* Electro-graphitization and exfoliation of graphene on carbon nanofibers. *Carbon* **117**, 201-207 (2017).

25. Vander Wal, R. L. *et al.* Carbon nanostructure examined by lattice fringe analysis of high-resolution transmission electron microscopy images. *Appl. Spectrosc.* **58**, 230-237 (2004).

26. Kim, D.-Y., Nishiyama, Y., Wada, M. & Kuga, S. Graphitization of highly crystalline cellulose. *Carbon* **39**, 1051-1056 (2001).

27. Haensel, T. *et al.* Pyrolysis of cellulose and lignin. *Appl. Surf. Sci.* **255**, 8183-8189 (2009).

28. Luo, B. *et al.* Chemical vapor deposition of bilayer graphene with layer-resolved growth through dynamic pressure control. *J. Mater. Chem. C* **4**, 7464-7471 (2016).

29. Li, J. *et al.* Controllable atmospheric pressure growth of mono-layer, bi-layer and tri-layer graphene. *Chem. Commun.* **50**, 11012-11015 (2014).

30. Jalilov, A. S. *et al.* Mechanistic study of the conversion of superoxide to oxygen and hydrogen peroxide in carbon nanoparticles. *ACS Appl. Mater. Interfaces* **8**, 15086-15092 (2016).

31. Moghaddam, S. E. *et al.* Morphogenesis of cement hydrate. *J. Mater. Chem. A* **5**, 3798-3811 (2017).

32. Hosseini, E., Zakertabrizi, M., Korayem, A. H. & Shahsavari, R. Tunable, multifunctional ceramic composites via intercalation of fused graphene boron nitride nanosheets. *ACS Appl. Mater. Interfaces* **11**, 8635-8644 (2019).